

KINEMATIC AND DYNAMIC ANALYSIS OF MOBILE ROBOT

MAUNG THAN ZAW

NATIONAL UNIVERSITY OF SINGAPORE

2003

KINEMATIC AND DYNAMIC ANALYSIS OF MOBILE ROBOT

MAUNG THAN ZAW
(B.Eng (Electronics), M.Sc (Mechatronics))

A THESIS SUBMITTED
FOR THE DEGREE OF MASTER OF SCIENCE
DEPARTMENT OF COMPUTER SCIENCE
NATIONAL UNIVERSITY OF SINGAPORE

2003

Acknowledgements

First and foremost, I would like to express my sincere gratitude to my former supervisor Prof. Sung Kah Kay.

I am deeply indebted to my supervisor Dr. Ng Teck Khim for his guidance, patient and support. Without his continued support and encouragement, this work would not have been possible.

I would also like to thank my co-supervisor A/P Marcelo H. Ang, Jr. for his guidance and advices. I am indebted to Prof. Oussama Khatib for his providing valuable advices and ensuring that I am on the right track.

I am grateful to Dr. Lim Ser Yong for his support and I would like to thank my colleagues Denny Oetomo, Xia Qinghua, Mana Saedan, Chee Wang and some colleagues from SIMTech.

Finally, I would like to thank School of Computing, National University of Singapore for financial support of the Research Scholarship.

Table of Contents

Acknowledgement	i
Table of Contents	ii
Summary	iv
List of Figuresvi
List of Tablesviii
1. Introduction	1
1.1 Research Background	1
1.2 Motivations and Objective	2
1.3 Contributions	5
1.4 Outline of the thesis	6
2. Related Work	7
2.1 Review of Different Kinds of Mobile Base	7
2.2 Kinematic and Dynamic Modeling of Mobile Base	12
2.3 Kinematic and Dynamic Analysis	16
2.3.1 Kinematic Analysis	16
2.3.2 Dynamic Analysis	17
2.3.3 Conclusion	18
3. Kinematic Modeling and Analysis	19
3.1 Kinematic Modeling	19

3.1.1	Kinematic Modeling of Single Wheel	19
3.1.2	Kinematic Modeling of Mobile Robot	23
3.2	Kinematic Analysis	27
3.3	Condition Number Polar Plot (CNPP)	32
3.4	Simulation of Four Wheels Mobile Robot	35
4.	Dynamic Modeling and Analysis	41
4.1	Dynamic Modeling	42
4.2	Dynamic Analysis	48
5.	Conclusions	74
5.1	Summary	74
5.2	Recommendation and Future Work	75
	References	77
	Appendix A. Design of Powered Caster Wheel Module	85
A.1	Computation for Rolling Torque	85
A.2	Computation for Steering Torque	86
A.3	Computation for motor specifications	87
	Appendix B. Drawings of Caster Wheel Module	89

Summary

Mobile robots with omni-directional motion capabilities are very useful. These robots have the ability to independently translate along a horizontal plane and rotate about a vertical axis (i.e., three independent degrees of freedom for motion of the mobile base). Such capabilities will pave the way towards much more applications, especially mobile manipulation capabilities in spaces require full maneuverability.

In this thesis, we present the kinematics of one class of omni-directional mobile robots, whose designs are motivated by 2-axis powered caster wheels with non-intersecting axes of motion. Complete kinematics of the wheel and the base are completely derived using Denavit-Hartenberg parameterization. Our derivation differs from the conventional approach where the Jacobian of the wheel and base are derived directly from velocity transformations and constraints. Our approach treats the caster wheel as a serial robot and is physically intuitive.

The kinematics analysis is carried out by analyzing the condition number of Jacobian matrix. The condition number of Jacobian as a measure of kinematics performance is introduced by (Salisbury and Craig, 1982).

The dynamic of single wheel is derived from the serial robot model and multi-wheel mobile robot is derived using the operational space approach and augmented object model introduced by (Khatib, 1987). We have formulated the theorem of “Dynamically Isotropic Configuration” as a supplementary tool for augmented object model in operational space.

The dynamic analysis is carried out by analyzing the condition number of operational space pseudo kinetic energy matrix, and further analysis is carried out by utilizing the *Generalized Inertia Ellipsoid* (GIE) introduced by (Asada, 1983).

The results of our analysis show that in kinematic, the wheel offset b must not equal to zero. In dynamic, in order to achieve dynamic isotropy, two identical wheels must be fixed 90° apart, whereas for more than two identical wheels, polar symmetry configuration must be observed.

List of Figures

2.1	Steered conventional wheels	9
2.2	Omnidirectional wheels	10
2.3	Special wheels	11
3.1	An instantaneous kinematic model of caster wheel	20
3.2	Multi wheel mobile robot	23
3.3	Condition numbers of single wheel in different steering angles	28
3.4	Effect of radius of the base on condition number of Jacobian matrix	29
3.5	Three different wheel configurations of mobile robot	30
3.6	The plot of condition number of three wheels in three different directions ..	30
3.7	Velocity ellipsoids of single wheel in different steering angles	31
3.8	Two links manipulator	32
3.9	CNPP of two links manipulator	33
3.10	CNPP of (a) single wheel (b) three wheels (c) four wheels	34
3.11	Simulation of four wheels mobile robot with applied velocity in x direction .	35
3.12	Initial and final position of four wheels mobile robot	35
3.13	Simulation of four wheels mobile robot with applied velocity in y direction .	37
3.14	Initial and final position of four wheels mobile robot	37
3.15	Simulation of four wheels mobile robot with applied angular velocity	39
3.16	Initial and final position of four wheels mobile robot	39

4.1	Dynamic model of a wheel module with three actuators	42
4.2	Inertia models for three links of caster wheel module	46
4.3	Condition number of single wheel translational pseudo kinetic energy matrix	49
4.4	Effect of radius of the mobile base on condition number of $\Lambda_{vi}(q)$	50
4.5	Three wheels mobile robot in three different directions	53
4.6	The plot of condition number of three wheels in three different directions . .	53
4.7	Four wheels mobile robot in three different directions	54
4.8	The plot of condition number of four wheels in three different directions . .	54
4.9	Five wheels mobile robot in three different directions	55
4.10	The plot of condition number of five wheels in three different directions . . .	55
4.11	Inertia ellipsoid	57
4.12	Inertia ellipsoid of single wheel in different steering angles	58
4.13	Inertia ellipsoid for translational motion of augmented mobile platform . . .	59
4.14	Inertia ellipsoids of the wheels in different configurations	65
4.15	The effect of number of identical wheels on the condition number of Λ . . .	66
4.16	Augmentation of ellipsoid in four wheels mobile robot	68
4.17	CNPP of four wheels	68
4.18	Effect of offset b on four wheels mobile robots	69
4.19	Effect of mass of link three on four wheel mobile robot	70
4.20	Two links manipulator	71
4.21	CNPP of two links manipulator	72
A.1	Powered Caster Wheel Module	87

List of Tables

3.1	D-H parameters	21
4.1	The ranges of the parameters of interest	47

Chapter 1

Introduction

1.1 Research Background

Wheeled mobile robots (WMRs) have been an active area of research and development over the past three decades. This long-term interest has been mainly inspired by many practical applications that can be uniquely addressed by mobile robots due to their ability to work in large (potentially unstructured and hazardous) domains. Specially, WMRs have been employed for applications such as: industry, hospitals, education, rescue, mine detection, monitoring nuclear facilities and warehouses for material inspection and security objectives, planetary exploration, military tasks such as munitions handling, materials transportation, vacuum cleaner, automatic guided vehicle exploration and entertainment. Based on the wide range of applications described above, it is clear that WMR research is multidisciplinary by nature.

Mobile robots are always categorized into two groups: wheeled-robots and legged-robots. Legged-robots have advantage over wheeled-robots for moving on very rough surface. For smooth surface, wheeled-robots are always quicker than legged-robots. Wheeled-robots have no problem of stability or balance as always occurred in legged-robots. Wheeled mobile robots (WMRs) are more energy efficient than legged robot on hard,

smooth surfaces; and will potentially be the first mobile robots to find widespread application in industry, because of the hard, smooth plant floors in existing industrial environments. WMRs require fewer and simpler parts and are thus easier to build than legged mobile robots. Wheel control is less complex than the actuation of multi-joint legs.

1.2 Motivations and Objective

Motivation for Kinematic and Dynamic Modeling

Many researchers have developed methodologies for the kinematic and dynamic modeling of wheeled mobile robots. An extensive study of this subject was published by (Muir, 1988). A three-wheeled 2-DOF mobile robot was modeled by (Saha and Angeles, 1989). (Alexander and Maddocks, 1989) studied the planar rigid-body motions which can be achieved for a given wheel configuration and the steering drive rates that access the motion. A particular case of three-wheeled robot (two-front wheel and one-rear wheeled) was modeled by (D'Andrea et al., 1991).

Kinematic and dynamic modeling of WMR can be classified under two types: vector approach (Wada and Mori, 1996), (Saha and Angeles, 1989), (Yi and Kin, 2002) and transformation approach (Muir and Numan, 1987c), (Holmberg, 2000), (Cheng and Rajagopalan, 1992). The vector approach is not generic. (Campion et al., 1996) reported a technique to classify WMRs to study the kinematic and dynamic models while taking into account the mobility restriction induce by constraints.

In particular, there is no standard formulation in kinematic modeling and dynamic modeling as in stationary robot manipulators. In the literature of stationary robot manipulator, kinematic and dynamic modeling are well established, for instance, in kinematic Denavit-Hartenberg parameters are used for coordinate transformations to obtain the kinematic model, and Lagrange and Newton-Euler are utilized to obtain the dynamic model. As such, using these methodologies in mobile robot will be the new exploration to bridge the two different literatures into one.

In literature, there are few published papers which are somewhat closer to this methodology. In fact, they are of transformation approach (Muir and Numan, 1987c) (Cheng and Rajagopalan, 1992). In particular, (Muir, 1988) derived the kinematic model of mobile robot using coordinate transformation, however, his approach involved extensive computation of matrix transformation and it is rather complicated. (Holmberg, 2000) reported using Denavit-Hartenberg parameterization but there is no detail derivation of kinematic and dynamic models of the mobile robot.

Therefore, this inspired us to derive the kinematic and dynamic models of the mobile robot based on Denavit-Hartenberg parameterization. The result of our work will be presented in this thesis somewhat similar to (Muir, 1988) and (Holmberg, 2000) but different in approach. In deriving our kinematic model, we first treated the single wheel as a serial link manipulator, and then the model of mobile robot is formulated using derived single wheel model. The dynamics of the wheel is formulated from the serial

robot model and dynamic of mobile robot is derived using augmented object model approach in operational space introduced by (Khatib, 1987).

Motivation for Kinematic and Dynamic Analysis

In analysis of robotic manipulator, the main tool that researchers have been using to quantify the kinematic performance of a manipulator is the analysis of its Jacobian matrix (Angeles, 1992a, 1992b), (Salisbury and Craig, 1982), (Paul and Stevenson, 1983), (Yoshikawa, 1985), (Klein and Blaho, 1987), (Kircanski, 1994) i.e., the matrix relating joint speeds to end-effector velocity. Many indices for kinematic performance have been proposed based on this matrix, for instance, condition number (Salisbury and Craig, 1982), the value of the determinant (Paul and Stevenson, 1983), manipulability (Yoshikawa, 1985) and minimum singular value (Klein and Blaho, 1987). To design robot manipulators for good kinematic performance is to select structural parameters that make the Jacobian matrix as isotropic as possible in the workspace (Angeles 1992a, 1992b), (Salisbury and Craig, 1982), (Kircanski, 1994). Then, for a given joint-speed norm, the velocity would be as uniform as possible in operational space.

On the other hand, dynamic performance can be characterized by the acceleration capability of the end-effector perceived at the end-effector (Asada, 1983) or at the actuators (Yoshikawa, 1985). This ability is indicated by matrices defined in (Asada, 1983) and (Yoshikawa, 1985).

In robotic literature, it has been paid less attention to kinematic and dynamic analysis of mobile robot. Using the methodologies from stationary robotic manipulator to analyze the performance of mobile robot would be the new exploration to achieve an optimal design.

1.3 Contributions

The contributions of this thesis are as follows.

Firstly, the new concept of kinematic model of caster wheel is formulated as a serial link manipulator by using Denavit-Hartenberg convention. As expected, our model is exactly the same as that of (Muir, 1988) which involves extensive computation of matrix transformation. The kinematic analysis is carried out using the methodologies from stationary robotic manipulator.

Secondly, the dynamic model of caster wheel is formulated as a serial link manipulator and the augmented object model (Khatib, 1987), (Williams and Khatib, 1993), (Holmberg, 2000) was utilized to represent the mobile robot as a system of cooperative robotic manipulators. The dynamic analysis is carried out using the methodologies from stationary robotic manipulator.

Thirdly, we have introduced the Condition Number Polar Plot (CNPP) (Zaw et al., 2003a), (Zaw et al., 2003b) to use as a tool for designing of mobile robot and which can also be used for particular joint of robotic manipulator of interest. This tool is applicable not only to kinematic but also to dynamic analysis.

Finally, we have formulated the theorem of “Dynamically Isotropic Configuration” as a supplementary tool for augmented object model in operational space introduced by (Khatib, 1987).

1.4 Outline of the Thesis

The outline of this thesis is as follows:

In this chapter, we have described the research background, motivations followed by the contributions of this thesis.

Chapter 2 provides a review of existing kinematic and dynamic models of mobile robot.

Chapter 3 is one of the two main chapters of thesis. We will first be presenting the kinematic modeling of mobile robot. This is followed by kinematic analysis.

Chapter 4 is the main chapter of this thesis. We will first be presenting the dynamic modeling of mobile robot. This is followed by dynamic analysis.

Chapter 5 concludes this thesis with some possible future work.

Chapter 2

Related Work

2.1 Review of Different Kinds of Mobile Bases

Wheeled mobile robots have been an active research area and developed over the past three decades. The advantages of these robots over the legged mobile robots are easy to manufacture, high pay load and high efficiency. These mobile robots fall into two categories; these are omnidirectional and non-omnidirectional. Omnidirectional mobile robot means it can maneuver in any direction on the ground plane at any instance of time whereas non-omnidirectional means there is a mechanical constraint at least in one direction. Of particular interest, because of its full maneuverability on the ground plane, omnidirectional mobile robot is chosen for our research project which will be addressed in detail in this thesis.

There are three different kinds of wheels utilized in designing of the omnidirectional mobile robot in literature. These are mobile robots using steered conventional wheels, omnidirectional wheels and special wheels.

In first type, there are two different kinds of wheels fall into this type, these are:

1. Steered conventional wheel (without offset)
2. Steered conventional wheel with offset (caster wheel)

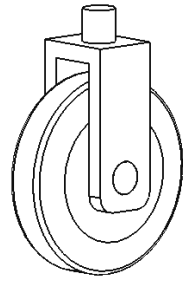
In second type, the following kinds of wheels fall into this type:

1. Universal omnidirectional wheel
2. Mecanum or Swedish wheel

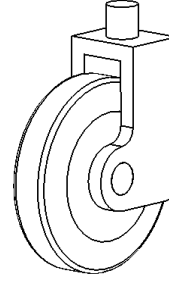
In last type, two different kinds of wheels can be found:

1. Orthogonal wheel
2. Ball wheel

The conventional wheel is probably the simplest wheel design. However, not all conventional wheels are capable of providing omnidirectional motion capability (Muir and Numan, 1987a), (Alexander and Maddocks, 1989), (Ostrovskaya et al., 1998). The steered conventional wheel is the wheel which is mounted on a rotational link and the vertical rotation axis of steering passes through the horizontal axis of wheel rotation. The caster wheel (Wada and Mori, 1996), (Ferriere et al., 1996) is the wheel with slight variation of first one that is its steering axis does not pass through axis of wheel rotation and there is a offset distance between vertical steering axis and the horizontal axis of wheel rotation. The advantage of having offset is it can avoid the mechanical constraint in lateral motion. It has been widely accepted that caster wheel design provides full mobility (Campion et al., 1996). An omnidirectional mobile robot using steered wheel with offset was proposed by (Wada et al., 1995).



Steered conventional wheel

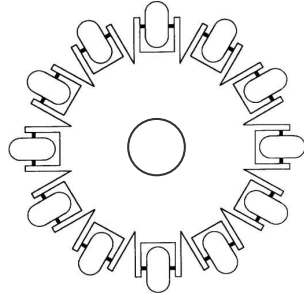


Steered conventional wheel with offset

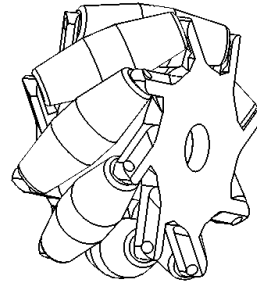
Figure 2.1: Steered conventional wheels

There has been a lot of effort in the development of omnidirectional wheels (Ferriere et al., 1996), (La et al., 1981), (Paromtchik and Rembold, 1994). The universal omnidirectional wheel is a disk with a multitude of conventional wheels or rollers mounted on its periphery. It achieves traction in one direction and allows passive motion in another direction. The drawback of this wheel is a generating of vibration when changing the contact points between the rollers and ground. Having big disk for forwards motion and small rollers for lateral motion, the speeds of the wheel are different in both motions therefore it causes vibration.

The Mecanum wheel design is based on similar concept (Muir and Numan, 1987b). It has angled passive rollers around the peripheral of the wheel. By controlling the four wheels attached to a platform, omnidirectional mobility can be achieved. In (Muir and Numan, 1987b), the mecanum wheels are utilized in their omnidirectional mobile robot, Uranus. Mecanum wheel has the problem that the small diameter of the roller, especially near the ends of the rollers, is limiting; and vibration caused by wheel speed variation.



Universal omnidirectional wheel



Mecanum wheel

Figure 2.2: Omnidirectional wheels

One of the special wheels is the orthogonal wheel developed by (Killough and Pin, 1992), (Pin and Killough, 1994). In orthogonal-wheel assembly, the major components are two spheres of equal diameter which have been sliced to get two parallel and equal plane surfaces. The axle of wheel passes through the centers of these parallel surfaces and both end of axel are held in a bracket using ball bearings so that the wheel is free to rotate around its axle. The two brackets are mounted orthogonally to each other on the axis of the main shaft. Both ends of the shaft are held in vertical plates with ball bearings. To provide the rotation of two wheels assembly, one end of the main shaft is connected to a motor so that contact with the ground is provided alternatively by one wheel or the other when the main shaft rotates. When the motor drives the main shaft, the wheels provide traction in the direction perpendicular to the main shaft while they are free to rotate in the direction parallel to main shaft. The advantages of this design over the universal wheels are fewer needed parts, smaller wheel size requirements and smoother contact with ground. This mechanism also suffers from vibration due to wheel speed variation as in the double universal wheel and they have low ground clearance.

The ball wheel was developed by (Ostrovskaya, 2000), (West and Asada, 1995, 1997). This ball wheel possesses three degree of freedom and good omnidirectional mobility, but its driving mechanism is complicated. In (West and Asada, 1995), they used active and passive rollers to guide and power the motions of the ball wheel. This design behaved much like an omnidirectional wheel with a driven direction of motion and a passive direction of motion. The ball wheel mobile robot is capable of smooth rolling motion with no wheel gaps and smooth varying wheel speed. In ball wheel drive mechanism, power from a motor is transmitted through gears to an active roller ring and then to the ball via friction between the rollers and the ball. Since it is being a friction driven mechanism, power transmitting to ball wheel is not efficient as other wheel designs. The robots with ball wheels can carry only limited load capacity and do not robust to dust and oil. The ball wheel mechanism has low clearance with the ground and the height of the obstacles is limited by the small diameter of the rollers. This ball wheel mechanism is therefore not robust to environment and it needs highly clean floor.

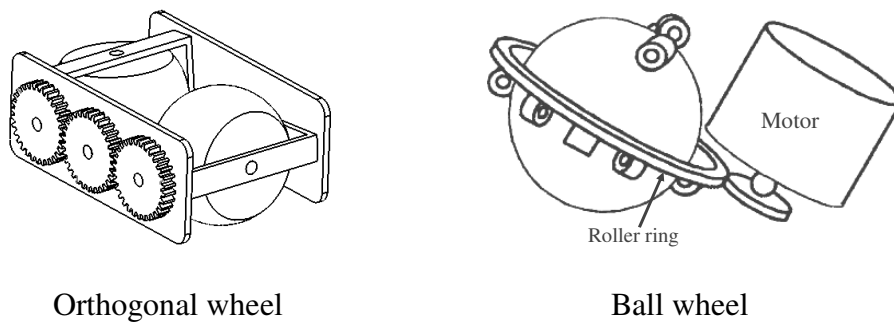


Figure 2.3: Special wheels

Among all the wheels, the steered conventional wheel with offset demonstrates to achieve omnidirectional mobility and non-redundancy properties. Moreover, it has high

clearance with the ground and robust to environment, therefore this wheel was chosen for our project.

2.2 Kinematic and Dynamic Modeling of Mobile Robot

In the literature of mobile robot, kinematic and dynamic modeling of WMR can be classified under two types. These are vector approach (Saha and Angeles, 1989), (Wada and Mori, 1996), (Yi and Kin, 2002) and transformation approach (Muir and Numan, 1987c), (Cheng and Rajagopalan, 1992), (Holmberg, 2000). The vector approach is not generic. (Campion et al., 1996) reported a technique to classify WMRs to study the kinematic and dynamic models while taking into account the mobility restriction induce by constraints.

In vector approach (Saha and Angeles, 1989), a coordinate frames of unit vector i, j, k is fixed at the centroid of the platform and e_i, f_i, g_i ($i=1, 2, 3$) are attached to the centers of the wheels, number 1, 2, and 3. With unit vectors defined, the velocity at centroid is computed. The angular velocity of the vehicle is obtained from joint rates of the driving wheels then the relationship between the velocity of the platform and the actuated joint rates is obtained. The twist of the platform, a 6D vector of the angular velocity of vehicle, is defined as a linear transformation of the actuated joint rate vector and then twist rate or acceleration of the platform is obtained by differentiating the twist.

In vector approach dynamic modeling, the concept of orthogonal complement is used to develop the dynamical equations of motion. The natural orthogonal component of the matrix of velocity constraints can be computed as follows:

In first step, the twist of a rigid body is defined then the Newton-Euler equations governing the motion of the body is formulated by defining the wrench acting on the body. In second step, it is assumed that the mechanical system under motion is composed of “p” rigid bodies, and the Newton-Euler equations for the i^{th} body are obtained. By defining $6p \times 6p$ matrices of generalized mass and of generalized angular velocity as well as the $6p$ -dimensional vectors of generalized twist of generalized wrench and generalized nonworking constraint wrench, a set of $6p$ unconstrained dynamical equations are obtained.

In third step, the kinematic constraints produced by nonholonomic coupling are derived in differential form. These constraints can be represented as a system of linear homogeneous equation on the twists. This is equivalent to $A\dot{t}=0$ (where A is a $(6r+3v) \times 6p$ matrix, r and v being the number of independent holonomic and nonholonomic constraints, respectively) linear system on the vector of generalized twist. Under the assumption that the degree of freedom of the system is “n”, a n -dimensional vector of independent or actuated generalized speeds is defined. From the generalized twist, T orthogonal component of A is obtained.

In step four, because of the definitions of A and the vector of nonworking constraint wrench, the latter turns out to lie in the range of the transpose of A and hence, the said wrench lies in the nullspace of the transpose of T . Therefore, upon multiplication of both sides of the $6p$ -dimensional Newton-Euler uncoupled equations of the system by the

transpose of T , the vector nonworking constraint wrench is eliminated from the said equation, which leads to system of n independent constrained dynamical equations is obtained. This represents the system's Euler-Lagrange dynamical equations, which appear free of constraint forces.

In transformation approach (Muir, 1988), he begins modeling a WMR by sketching the mechanical structure. Then he assigns one body coordinate system, and a hip, steering, and contact coordinate system for each wheel. He applies the Sheth-Uicker convention (Sheth and Uicker, 1971) to coordinate system assignment and transformation matrix computation because it allows the modeling of the higher-pair wheel contact point motion and provides unambiguous transformation matrix labeling for the multiple closed-chains formed by the wheels.

He models each wheel (conventional, steered-conventional, omnidirectional or ball wheel) as a planar-pair which allows three DOFs: x-direction, y-direction, and θ -rotation. A conventional wheel attains y-translational motion by rolling contact. The translation in the x-direction and the θ -rotation about the point-of-contact occur when the wheel slips. He models the rotational slip as a wheel DOF because relatively small forces are required. He does not consider the x-translational wheel slip a DOF because relatively large forces are necessary. Omnidirectional wheels rely on rotational wheel slip, whereas ball wheels do not.

By inspection of the sketch, he writes the body-to-hip, hip-to-steering, steering-to-contact, and body-to-contact transformation matrices for each wheel. Under the assumption of no translational wheel slip, the wheel rotations define the motion of the

wheel contact point coordinate system with respect to a stationary coordinate system at the same position and orientation on the floor. The coordinate system fixed with respect to the floor is important because he references the velocities of the wheel contact point to this instantaneously coincident coordinate system. The rotational velocity of a wheel about its axle is thus proportional to the translational velocity of the contact point coordinate system with respect to the instantaneously coincident wheel contact-point coordinate system. Similarly, there is an instantaneously coincident body coordinate system to reference the velocities of the body coordinate system. He assigns instantaneously coincident coordinate systems because of the higher-pair wheel contact points.

For each wheel he develops a Jacobian matrix to specify the WMR body velocities (in the instantaneous coincident body coordinate system) as linear combinations of the wheel velocities (e.g., the steering velocity, the rotational velocity about the wheel axle, the rotational slip velocity, and the roller velocities for omnidirectional wheels). He writes the Jacobian matrix for a wheel by substituting elements of the coordinate transformation matrices, wheel and roller radii and roller orientation angles into the symbolic Jacobian matrix templates.

In transformation approach (Muir, 1988), the dynamic model of a robotic mechanism is formulated by computing independently the force/torque equation-of-motion and the kinematic transformations. The kinematic transformations are substituted into the force/torque equation-of-motion to formulate a dynamic model which depends only upon

the accelerations of the main link and the sensed joint positions and velocities. The dynamic model is then solved for the actuator force/torque and for the WMR body accelerations.

2.3 Kinematic and Dynamic Analysis

2.3.1 Kinematic Analysis

The main aim of this section is to describe the optimal design methodologies currently available in designing of robotics manipulators to achieve the optimal performance and accuracy. The tool that researchers have proposed to quantify the kinematic performance of a manipulator is the analysis of its Jacobian matrix (Angeles, 1992a, 1992b), (Salisbury and Craig, 1982), (Paul and Stevenson, 1983), (Yoshikawa, 1985), (Klein and Blaho, 1987), (Kircanski, 1994) i.e., the matrix relating joint speeds to end-effector velocity. Many indices for kinematic performance have been proposed based on this matrix, for instance, condition number (Salisbury and Craig, 1982), the value of the determinant (Paul and Stevenson, 1983), manipulability (Yoshikawa, 1985) and minimum singular value (Klein and Blaho, 1987). Since Jacobian matrix linearly maps the joint velocities to end-effector velocities and is a structure dependent matrix, being isotropy of this matrix is important in designing of manipulator. If the Jacobian matrix is isotropic, each actuator provides equal effort in all directions of end-effector motions. The condition number is defined as the ratio of the maximum singular value $\sigma_{\max}(J)$ to minimum singular value $\sigma_{\min}(J)$ of Jacobian matrix, i.e.,

$$K(J) = \frac{\sigma_{\max}(J)}{\sigma_{\min}(J)} \quad (2.1)$$

When $K(J)$ is equal to 1, all singular values of Jacobian matrix are equal and the Jacobian matrix is said to be isotropic. To design robot manipulators for good kinematic performance is to select the structural parameters that make the Jacobian matrix as isotropic as possible in the workspace (Angeles, 1992a, 1992b), (Salisbury and Craig, 1982), (Kircanski, 1994). Then, for a given joint-speed norm, the velocity would be as uniform as possible in operation space. To analyze the performance of mobile robot in this thesis, we will make use of condition number of the Jacobian matrix, manipulability ellipsoid and condition number polar plot (CNPP) which will be introduced in next chapter.

2.3.2 Dynamic Analysis

In robotic literature, many researchers have reported the formulations of several performance measures (Asada, 1983), (Khatib and Burdick, 1987), (Graettinger and Krogh, 1988), (Desa and Kim, 1990) of robotic manipulators. Most of these measures are related to the acceleration capabilities of the end-effector. (Asada, 1983) has introduced the *Generalized Inertia Ellipsoid* (GIE). In his approach, if the GIE is isotropic, the equivalent inertia of the end-effector is the same in all the directions in operation space. (Yoshikawa, 1985) has defined dynamic manipulability and has proposed the *Dynamic Manipulability Ellipsoid* (DME). In his approach, if the DME is isotropic, the actuators can accelerate the end-effector equally “easily” in all the directions in operation space. (Khatib and Burdick, 1987) have defined the *Hyper-Parallelepiped of Acceleration* (HPA) and formulated a cost function to optimize the dynamic design of robotic manipulators. Isotropic accelerations were found by inscribing spheres in the HPAs.

(Graettinger and Krogh, 1988) have defined the *Acceleration Radius* and computed it as an optimization problem. (Desa and Kim, 1990) have dealt with non-linearities in an analytical fashion. They have derived expressions for isotropic acceleration and maximum acceleration for a 2R planar manipulator. (Ma and Angeles, 1990) introduced a different measure of dynamic performance of manipulator, based on the concept of *Dynamic Isotropy*. In this thesis, we will make use of Asada's GIE to analyze the dynamic performance of mobile robot.

2.4 Conclusion

In this chapter, we have presented three different kinds of wheels utilized in designing of mobile robot and have made some comparisons among them. Among all the wheels, the caster offset wheel demonstrates to achieve omnidirectional maneuverability and non-redundancy properties. Furthermore, it can carry high payload and it has high clearance with the ground and robust to environment, therefore this wheel was chosen for our project. In kinematic and dynamic modeling, two different kinds of approaches, namely, vector approach and transformation approach are described. Both approaches involve extensive computations. Therefore, in next chapter, we will present our approach utilizing Denavit-Hartenberg convention as in stationary serial link robotic manipulator. To analyze the kinematic performance of mobile robot in this thesis, condition number, manipulability ellipsoid, and condition number polar plot (CNPP) which will be introduced in next chapter, are utilized to analyze the wheel Jacobian matrix, whereas for dynamic performance, condition number, generalized inertia ellipsoid, and CNPP are utilized to analyze the translational pseudo kinetic energy matrix of the wheel.

Chapter 3

Kinematic Modeling and Analysis

3.1 Kinematic Modeling

3.1.1 Kinematic Modeling of Single Wheel

To date, many different kinds of kinematic modeling of the mobile robot have been reported by researchers (Muir and Numan, 1987a), (Ostrovskaya, 2000), (West and Asada, 1995). Our derivation differs from their approach where the Jacobian of the wheel and base are derived directly from velocity transformations and constraints. Our approach treats the caster wheel as a serial robot and mobile robot as an augmented object of serial robots. The advantages of our approach over other approaches are as follows: Denavit-Hartenberg parameters can be used for coordinate transformations to obtain the kinematic model, and Lagrange and Newton-Euler can be utilized to obtain the dynamic model as in (Asada, H. and Slotine, J. J. E., 1986), (Craig, J. J., 1989), (Fu, K. S. Gonzalez, R. C. and Lee, C. S. G., 1987), (Paul, R. P., 1981), (Sciavicco, L. and Siciliano, B., 1996). In formulation of our kinematic model, we treat the wheel module as a serial link manipulator with two revolute joints and one prismatic joint in instantaneous time so that this model exactly maps to the physical wheel module in instantaneous time. The point of wheel contact with the floor is taken as a revolute joint (σ) since the wheel twists on the

floor but this joint is passive joint with no position feedback (no odometry). With the assumption of wheel rolling without slipping, wheel rolling is treated as a prismatic joint ($r\rho$) since angular and linear displacement of the wheel are linearly related. ($d = r\rho$ where r is radius and ρ is angular displacement of the wheel). And the steering joint is the last revolute joint (ϕ) of the system.

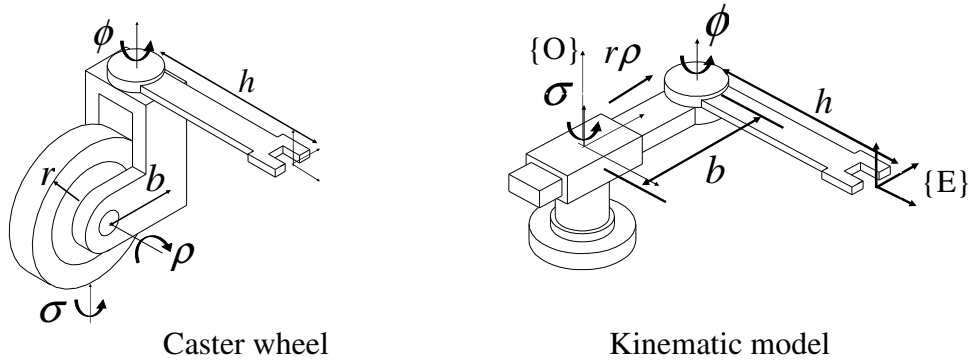


Figure 3.1: An instantaneous model of caster wheel

The wheel Jacobian is computed using Denavit-Hartenberg (D-H) parameterization as in serial manipulator (Craig, J. J., 1989). In Figure 3.1, the instantaneous base frame which moves together with the wheel is attached to the contact point between the wheel and the floor. From the frame assignments of the robot, we can obtain the following D-H parameters. In fact, since this manipulator has only three joints, the wheel Jacobian can be derived directly from the geometry of robot. D-H parameters however are used to formalize and to demonstrate its applicability.

By instantaneous, we mean that the prismatic joint($r\rho$) provides an instantaneous linear translation that pushes the end-effector forward with respect to the floor. At the same time, the mechanism has a set length of b (the wheel offset) between the rotation axes of σ and ϕ . The D-H parameter for the single caster wheel modeled as a serial manipulator

is shown in Table 3.1. The frame $\{O\}$ is an instantaneous frame that is always parallel to the world (absolute) frame, but moves together with the wheel. In other words, it is attached to the contact point between the wheel and the floor.

Joint i	α_i	a_i	θ_i	d_i
1	$-\pi/2$	0	σ	0
2	$\pi/2$	0	0	$r\rho$
3	0	0	ϕ	h

Table 3.1: Denavit-Hartenberg parameters (Denavit, J., and Hartenberg, R. S., 1955)

where h is radius of the mobile base. The position of the end-effector with respect to the base Frame $\{O\}$ in cartesian coordinate is:

$${}^0p_E = \begin{bmatrix} r\rho C_\sigma + hC_{\sigma+\phi} \\ r\rho S_\sigma + hS_{\sigma+\phi} \\ 0 \end{bmatrix} \quad (3.1)$$

where $C_\sigma = \cos(\sigma)$, $C_{\sigma+\phi} = \cos(\sigma + \phi)$, $S_\sigma = \sin(\sigma)$, $S_{\sigma+\phi} = \sin(\sigma + \phi)$

When differentiated, the position vector x will provide the velocity vector of the end-effector. Note that when differentiating $r\rho$ with respect to σ and ϕ , it is taken as the constant value of the offset b , which is the real physical distance. However, when differentiating $r\rho$ with respect to ρ , it is taken as variable with respect to time. Adding the rotational components (the rotational axes of σ and ϕ) into the Jacobian matrix, we obtain:

$${}^0J_E = \begin{bmatrix} -hS_{\sigma+\phi} - r\rho S_\sigma & rC_\sigma & -hS_{\sigma+\phi} \\ hC_{\sigma+\phi} + r\rho C_\sigma & rS_\sigma & hC_{\sigma+\phi} \\ 1 & 0 & 1 \end{bmatrix} \quad (3.2)$$

In derived Jacobian, $r\rho$ is set to physical offset distance b to maintain the physical model since our model is correct only at instantaneous time. Therefore, in instantaneous time

link two where $r\rho$ is assigned prismatic joint but in continuous time it is offset distance b . The reason being that is the base frame $\{O\}$ is following with manipulator caster wheel. The J matrix after setting $r\rho=b$ is:

$${}^0J_E = \begin{bmatrix} -hS_{\sigma+\phi} - bS_{\sigma} & rC_{\sigma} & -hS_{\sigma+\phi} \\ hC_{\sigma+\phi} + bC_{\sigma} & rS_{\sigma} & hC_{\sigma+\phi} \\ 1 & 0 & 1 \end{bmatrix} \quad (3.3)$$

where

$$\dot{X} = \begin{pmatrix} \dot{x} \\ \dot{y} \\ \dot{\theta} \end{pmatrix} = J \begin{pmatrix} \dot{\sigma} \\ \dot{\rho} \\ \dot{\phi} \end{pmatrix}$$

This is the Jacobian matrix with respect to Frame $\{O\}$. Notice that the Jacobian is a function of σ and ϕ . Since σ is not a measurable nor controllable variable, it is desired to have a Jacobian matrix that is not function of σ . This is obtained by expressing the Jacobian with respect to the end-effector frame (Frame $\{E\}$ in Figure 3.1)

To do so, the Jacobian is pre-multiplied by a rotational matrix:

$${}^EJ_E = {}^ER_0 \cdot {}^0J_E \quad (3.4)$$

where ER_0 is a rotation matrix derived from angle $\sigma + \phi$.

The resulting Jacobian for a single wheel module with respect to Frame $\{E\}$ is:

$${}^EJ_E = \begin{bmatrix} bS_{\phi} & rC_{\phi} & 0 \\ bC_{\phi} + h & -rS_{\phi} & h \\ 1 & 0 & 1 \end{bmatrix} \quad (3.5)$$

which is function of steering angle and contains design parameters b , r and h . Therefore, forward kinematic equation of single wheel is

$$\dot{X} = {}^EJ_E \dot{q} \quad (3.6)$$

and equation of inverse kinematic is

$$\dot{q} = {}^E J_E^{-1}(q) \dot{X} \quad (3.7)$$

Having derived the Jacobian of the single caster wheel, the next step is to derive the kinematic of the mobile robot in the following section.

3.1.2 Kinematic Modeling of Mobile Robot

In the case of multi wheel mobile robot, to find the Jacobian matrices of the rest of the wheels, it is only necessary to express them in the common frame (Frame {B}), which is attached to the center of the base:

$${}^B J_{Ei} = {}^B R_{Ei} {}^E J_{Ei} \quad (3.8)$$

where i denotes the caster wheel of interest, N is total number of wheel module in the mobile base and ${}^B R_{Ei}$ is the rotation matrix derived from angle β , as shown in Figure 3.2.

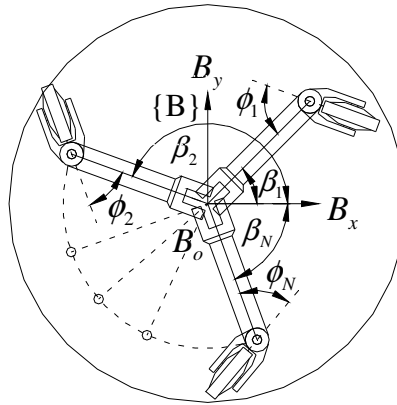


Figure 3.2: Multi wheel mobile robot

This result in the Jacobian of wheel i with respect to common Frame {B} at the center of the mobile base:

$${}^B J_{Ei} = \begin{bmatrix} hS_{\beta_i} + bS_{\beta_i + \phi_i} & rC_{\beta_i + \phi_i} & hS_{\beta_i} \\ hC_{\beta_i} + bC_{\beta_i + \phi_i} & -rS_{\beta_i + \phi_i} & hC_{\beta_i} \\ 1 & 0 & 1 \end{bmatrix} \quad (3.9)$$

and

$${}^B J_{Ei}^{-1} = \frac{1}{rb} \begin{bmatrix} rS_{\beta_i + \phi_i} & rC_{\beta_i + \phi_i} & -rhC_{\phi_i} \\ bC_{\beta_i + \phi_i} & -bS_{\beta_i + \phi_i} & bhS_{\phi_i} \\ -rS_{\beta_i + \phi_i} & -rC_{\beta_i + \phi_i} & r(b + hC_{\phi_i}) \end{bmatrix} \quad (3.10)$$

This derivation yields the same result as the vector approach found in (Yi and Kin, 2002) and transformation approach found in (Muir, 1988), (Holmberg, 2000). Note that the inverse always exists for $rb \neq 0$.

Forward Kinematics

In the expression of the Jacobian matrix (Equation 3.9), we assume that we are able to obtain the joint variable σ for the purpose of forward kinematics. In the real application, σ is not measurable.

In the inverse kinematics, however, it is possible to remove the σ component (see Equation 3.10). The inverse of Jacobian matrix without the σ component for any wheel i is obtained by simply removing the first row of ${}^B J_{Ei}^{-1}$. Therefore,

$${}^B \bar{J}_{Ei}^{-1} = \frac{1}{rb} \begin{bmatrix} bC_{\beta_i + \phi_i} & -bS_{\beta_i + \phi_i} & bhS_{\phi_i} \\ -rS_{\beta_i + \phi_i} & -rC_{\beta_i + \phi_i} & r(b + hC_{\phi_i}) \end{bmatrix} \quad (3.11)$$

which means

$$\begin{bmatrix} \dot{\rho}_i \\ \dot{\phi}_i \end{bmatrix} = {}^B \bar{J}_{Ei}^{-1} \begin{bmatrix} \dot{x} \\ \dot{y} \\ \dot{\theta} \end{bmatrix} \quad (3.12)$$

The Jacobian inverse of all the individual wheel modules can be combined to form an augmented Jacobian inverse \bar{J}_{aug}^{-1} :

$$\underbrace{\begin{bmatrix} \dot{\rho}_1 \\ \dot{\phi}_1 \\ \dot{\rho}_2 \\ \dot{\phi}_2 \\ \vdots \\ \dot{\rho}_N \\ \dot{\phi}_N \end{bmatrix}}_{\dot{q}_{aug}} = \underbrace{\begin{bmatrix} {}^B \bar{J}_{E1}^{-1} \\ {}^B \bar{J}_{E2}^{-1} \\ \vdots \\ {}^B \bar{J}_{EN}^{-1} \end{bmatrix}}_{\bar{J}_{aug}^{-1}} \underbrace{\begin{bmatrix} \dot{x} \\ \dot{y} \\ \dot{\theta} \end{bmatrix}}_{\dot{X}} \quad (3.13)$$

$$\text{where } \bar{J}_{aug}^{-1} = \frac{1}{rb} \begin{bmatrix} bC_{\beta_1+\phi_1} & -bS_{\beta_1+\phi_1} & bhS_{\phi_1} \\ -rS_{\beta_1+\phi_1} & -rC_{\beta_1+\phi_1} & r(b+hC_{\phi_1}) \\ bC_{\beta_2+\phi_2} & -bS_{\beta_2+\phi_2} & bhS_{\phi_2} \\ -rS_{\beta_2+\phi_2} & -rC_{\beta_2+\phi_2} & r(b+hC_{\phi_2}) \\ \vdots & \vdots & \vdots \\ bC_{\beta_N+\phi_N} & -bS_{\beta_N+\phi_N} & bhS_{\phi_N} \\ -rS_{\beta_N+\phi_N} & -rC_{\beta_N+\phi_N} & r(b+hC_{\phi_N}) \end{bmatrix}$$

The forward kinematic can be obtained by solving for $(\dot{x}, \dot{y}, \dot{\theta})^T$ from Equation 3.13, which represents a $2N$ equations ($N \geq 2$), for which in general, there may not be a solution. But in this case, the wheel modules are held together by physical constraints:

$$\begin{bmatrix} \dot{x} \\ \dot{y} \\ \dot{\theta} \end{bmatrix} = {}^B J_{E1} \begin{bmatrix} \dot{\sigma}_1 \\ \dot{\rho}_1 \\ \dot{\phi}_1 \end{bmatrix} = {}^B J_{E2} \begin{bmatrix} \dot{\sigma}_2 \\ \dot{\rho}_2 \\ \dot{\phi}_2 \end{bmatrix} = \dots = {}^B J_{EN} \begin{bmatrix} \dot{\sigma}_N \\ \dot{\rho}_N \\ \dot{\phi}_N \end{bmatrix} \quad (3.14)$$

therefore an exact solution exists using the left pseudo inverse of \bar{J}_{aug}^{-1} , i.e.:

$$J_{LPI} = ((\bar{J}_{aug}^{-1})^T \bar{J}_{aug}^{-1})^{-1} (\bar{J}_{aug}^{-1})^T \quad (3.15)$$

where

$$\begin{bmatrix} \dot{x} \\ \dot{y} \\ \dot{\theta} \end{bmatrix} = J_{LPI} \begin{bmatrix} \dot{\rho}_1 \\ \dot{\phi}_1 \\ \dot{\rho}_2 \\ \dot{\phi}_2 \\ \vdots \\ \dot{\rho}_N \\ \dot{\phi}_N \end{bmatrix} \quad (3.16)$$

In the case of single wheel, the Jacobian can be obtained using right pseudo inverse of

${}^B\bar{J}_{Ei}^{-1}$ as follows:

$$J_{RPI} = ({}^B\bar{J}_E^{-1})^T (\bar{J}_E^{-1} (\bar{J}_E^{-1})^T)^{-1} \quad (3.17)$$

where

$$\begin{bmatrix} \dot{x} \\ \dot{y} \\ \dot{\theta} \end{bmatrix} = J_{RPI} \begin{bmatrix} \dot{\rho} \\ \dot{\phi} \end{bmatrix}$$

Note that J_{LPI}^{-1} always exists for $rb \neq 0$. When the operation space velocity command vector is obtained from the control law, it can be use immediately used in Equation 3.13 to produce the joint rate command vector to be sent out to the high level controller for each joint to obtain the desired motion.

3.2 Kinematic Analysis

The condition number of Jacobian as a measure of kinematic performance was introduced by (Salisbury and Craig, 1982). In general, the condition number is a measure of how close a matrix is to being singular. The condition number [see also (Strang, G., 1993), (Golub, G. and Van Loan, C., 1989)] is defined as the ratio of the maximum singular value $\sigma_{\max}(J)$ to minimum singular value $\sigma_{\min}(J)$ of Jacobian matrix, and it is also related to eigenvalue (λ) of JJ^T , i.e.

$$K(J) = \frac{\sigma_{\max}(J)}{\sigma_{\min}(J)} = \frac{\sqrt{\lambda_{\max}(JJ^T)}}{\sqrt{\lambda_{\min}(JJ^T)}} \quad (3.18)$$

When $K(J)$ is equal to 1, all singular values of Jacobian matrix are equal and the Jacobian matrix is said to be isotropic.

Since Jacobian linearly maps the joint velocities to end-effector velocities and is a structure dependent matrix, being isotropy of this matrix is important in designing of manipulator. If the Jacobian matrix is isotropic, each actuator provides equal effort in end-effector motion in all directions. In the case of caster module, the design parameters to be taken into consideration are wheel radius, offset distance and radius of the platform. In order to obtain the isotropic Jacobian, aforementioned wheel parameters are verified by analyzing the condition numbers of the Jacobian.

In the case of single wheel, the condition number of Jacobian matrix in (3.15) is analyzed in the follows.

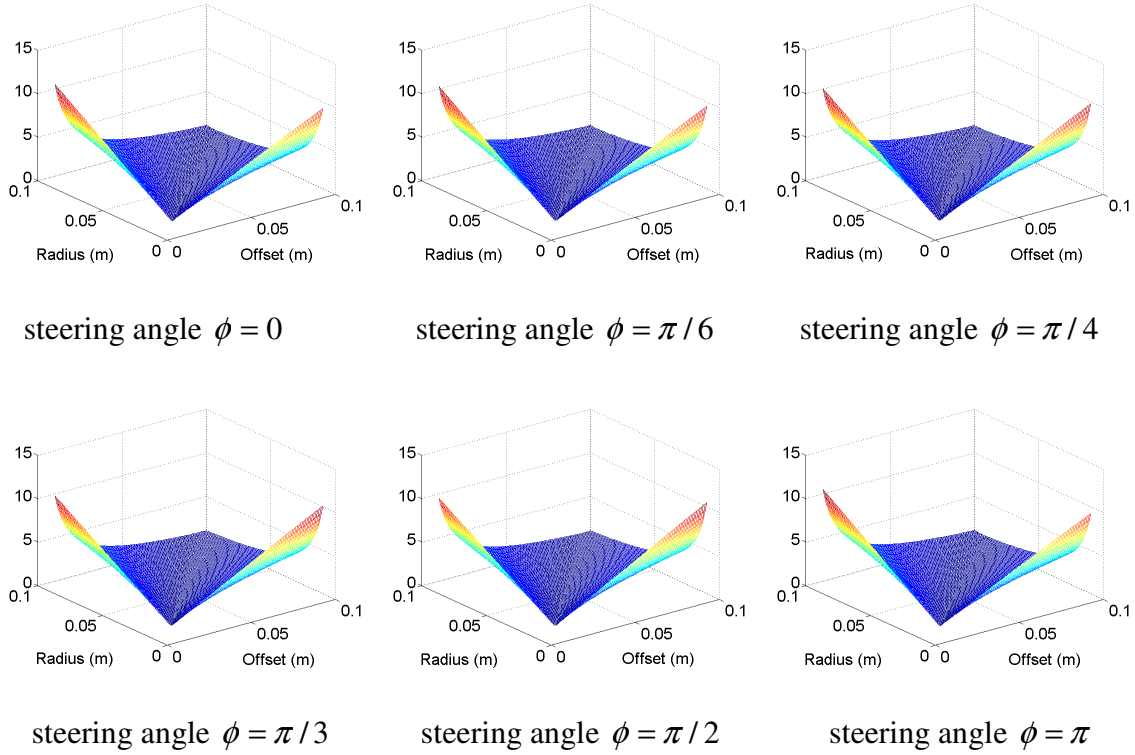


Figure 3.3: Condition numbers of single wheel in different steering angles

As shown in Figure 3.3, the condition number of the single wheel Jacobian varies with design parameters wheel radius and offset but varies slightly with steering angle. The pattern of the plot of condition number between 0° and 90° is exactly the same as that of between 90° and 180° . Therefore, in what follows, the analysis is carried out in the former range. As can be seen from figure, the condition number is sensitive only two regions which are of the range between small wheel radius (less than 0.02m) and entire offset, and the range between small offset (less than 0.02m) and entire wheel radius. The good region for the design parameter is (offset) $b \geq 0.02$ (m) and (radius) $r \geq 0.02$ (m). It is obvious that there is no significant effect of steering angle on the Jacobian we therefore left out to analysis this effect in the following kinematic analysis.

Effect of Base Radius of the Mobile Robot

It being one of the links in our model, the radius of the mobile robot is analyzed so as to see its effect on the performance in kinematic sense. In performing analysis, the condition number of the Jacobian is plotted by letting the radius vary. Of particular interest, the range of this value is between 0.2m and 0.4m.

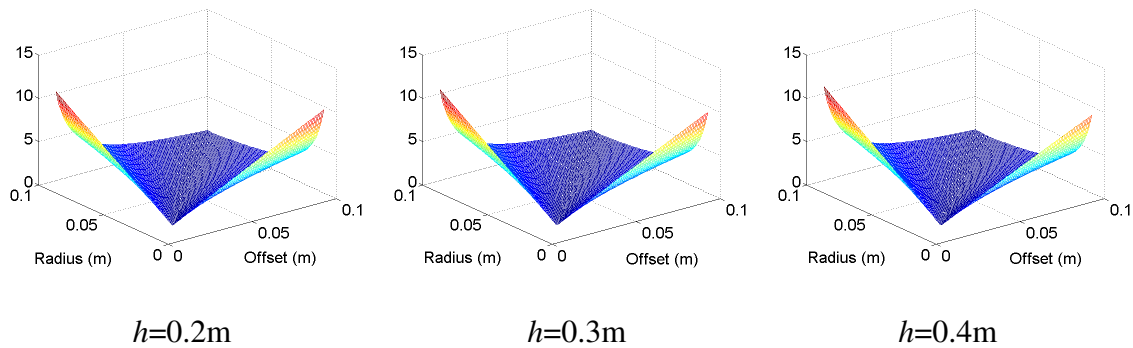


Figure 3.4: Effect of radius of the base on condition number of Jacobian matrix

The results show that the condition number of the wheel Jacobian does not vary much when the radius of the mobile robot varies.

Effect of number of wheels

When designing the mobile robot, the number of wheels to be used is taken into consideration. The same as previous, this analysis can be carried out by analyzing the condition number of the Jacobian matrix while varying this number. In our analysis, three different wheel configurations are considered they are of three wheels, four wheels and five wheels respectively.

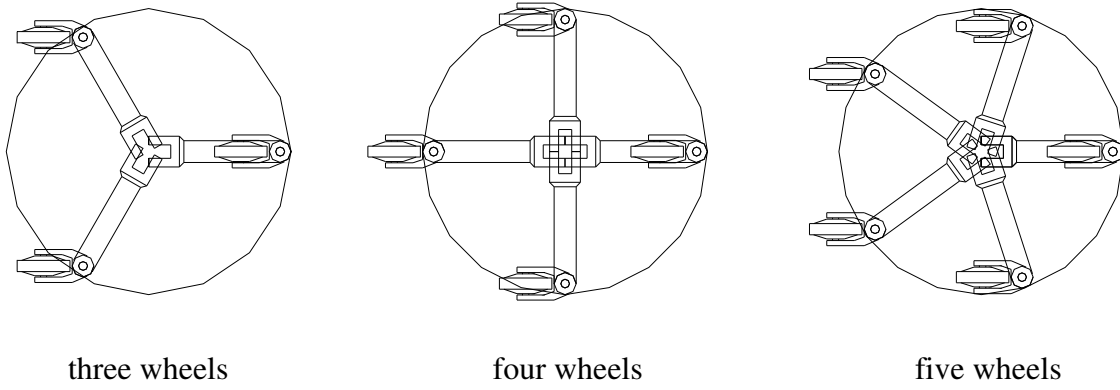


Figure 3.5: Three different wheel configurations of mobile robot

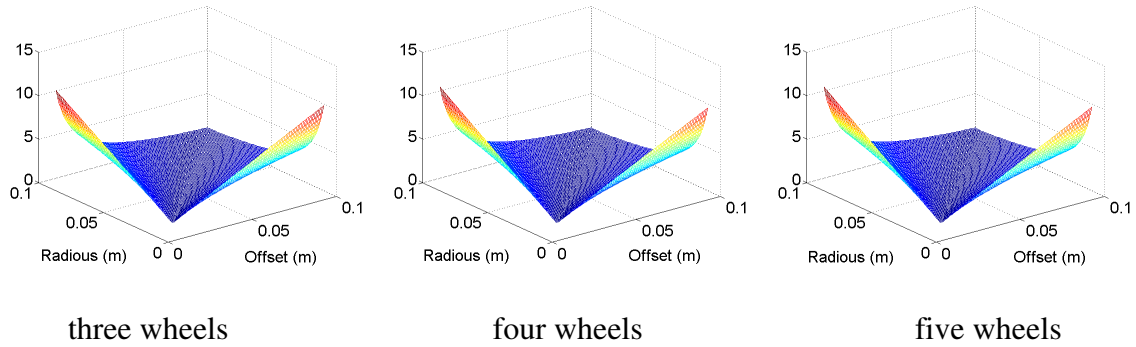


Figure 3.6: The plot of condition number of three different wheel configurations

As can be seen from Figure 3.6, the condition numbers of three different wheel configurations are almost the same.

Manipulability Ellipsoid

The condition number however describes only the ratio but not magnitude of the singular values or eigenvalues. In order to analyze and to visualize the kinematic performance, velocity manipulability ellipsoid is used in sequel. To measure the manipulating ability of the manipulator was first introduced by (Yoshikawa, 1985). According to his concept, the

velocity manipulability ellipsoid can be defined for the single wheel. The Jacobian ${}^B\bar{J}_{Ei}$ defines the mapping from joint space to operational space. If the unit sphere in joint space is described by

$$\|\dot{q}_i\|^2 = \dot{q}_i^T \dot{q}_i = 1 \quad (3.19)$$

this can be mapped to ellipsoid in operational space through ${}^B\bar{J}_{Ei}$ as

$$\dot{X}_i^T ({}^B\bar{J}_{Ei}^+)^T {}^B\bar{J}_{Ei}^+ \dot{X}_i = 1 \quad (3.20)$$

$$\dot{X}_i^T ({}^B\bar{J}_{Ei} {}^B\bar{J}_{Ei}^T)^{-1} \dot{X}_i = 1 \quad (3.21)$$

The velocity ellipsoid will have principal axes in the direction v_i , with magnitudes $\sqrt{\lambda_i}$, where v_i and λ_i are the eigenvectors and eigenvalues of ${}^B\bar{J}_{Ei} {}^B\bar{J}_{Ei}^T$. The velocity ellipsoids of the single wheel in different steering angles are shown in Figure 3.6.

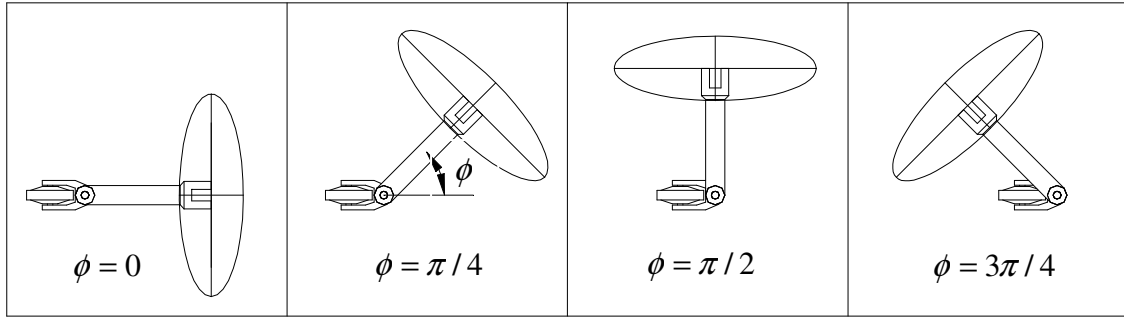


Figure 3.7: Velocity ellipsoids of single wheel in different steering angles

The values of parameters b , r and h for Figure 3.7 are of 0.02m, 0.06m and 0.325m respectively. As shown in figure, the velocity ellipsoid of single wheel does not vary with steering angles and it has at all no isotropy configurations.

3.3 Condition Number Polar Plot (CNPP)

The condition number polar plot can provide us more detail information about the performance of the revolute joint in 2D plane. In this plot, condition number is represented as a single line radial length and the polar angle is the joint angle of interest. This plot can be used as a tool to visualize not only isotropy but also singularity of the particular joint. As we described in previous section, the condition number is the ratio of maximum singular value to minimum singular value so that when minimum singular value becomes zero the condition number is infinity. Therefore, the length of the line representing this condition number will be very long in this plot. As an example, two links manipulator and caster wheel model are used to present as follows.

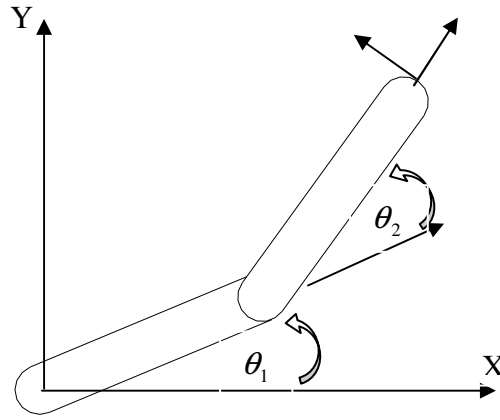


Figure 3.8: Two links manipulator

The Jacobian matrix of the two links manipulator is:

$$J_v = \begin{bmatrix} -l_1 \sin \theta_1 - l_2 \sin(\theta_1 + \theta_2) & -l_2 \sin(\theta_1 + \theta_2) \\ l_1 \cos \theta_1 + l_2 \cos(\theta_1 + \theta_2) & l_2 \cos(\theta_1 + \theta_2) \end{bmatrix} \quad (3.22)$$

In plotting the condition numbers of this two links manipulator, we fixed the angle of first link at 0° and then the angle of link 2 is varied. The resulting plot is shown in Figure 3.9.

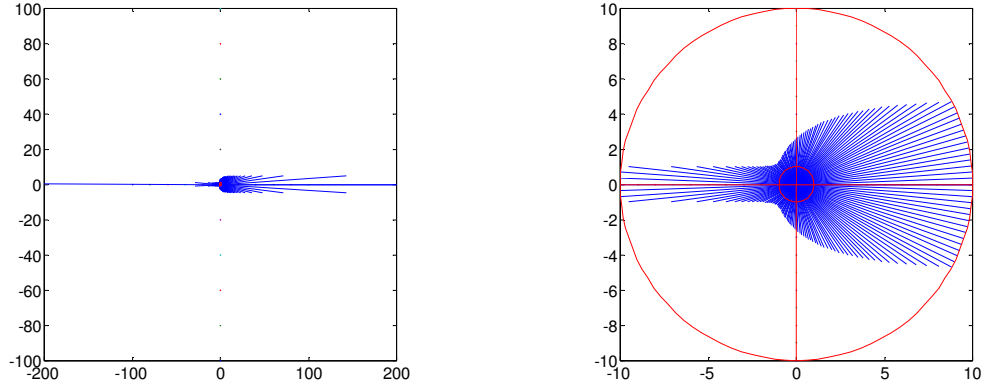


Figure 3.9: (a) CNPP of two links manipulator

(b) Close up view of isotropy and singular region

As can be seen from Figure 3.9(a), the Jacobian matrix (3.22) is singular at 0° and 180° of second link therefore the condition number is very large at these angles. For simplicity and clarity, we limited the condition number at singularity region to be of 10 in Figure (b) as close up view. Therefore, in the Figure 3.9(b), the outer circle represents the singularity while inner unit circle represents the isotropy of the manipulator. It is obvious that, for ideal case, if the isotropy is achieved then there would be no singularity.

We analyze the kinematic performance of caster wheel using CNPP in Figure 3.10.

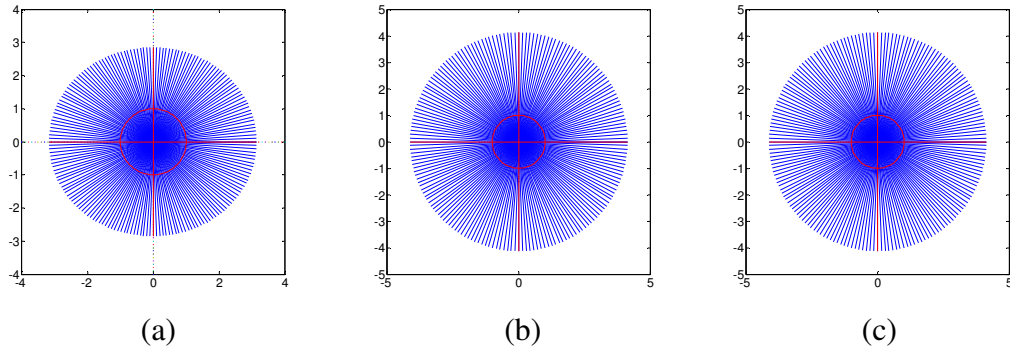


Figure 3.10: CNPP of (a) single wheel (b) three wheels (c) four wheels

With other two joints fixed, the CNPP is obtained by letting the steering angle vary. Figure 3.10 shows that there is no isotropy condition or singular condition over the entire range of steering angle. It should also be noted that apart from the single wheel, performance of the mobile robot with three wheels or four wheel configurations are slightly better in the sense that their condition numbers span equally over the entire range of steering angle. In the case of single wheel, the condition numbers in x and y are slightly different therefore the efforts to move the single wheel module are slightly different in both directions.

3.4 Simulation of Four Wheels Mobile Robot

To verify the correctness of the model we derived, the simulations were carried out and the results are shown in the figure below.

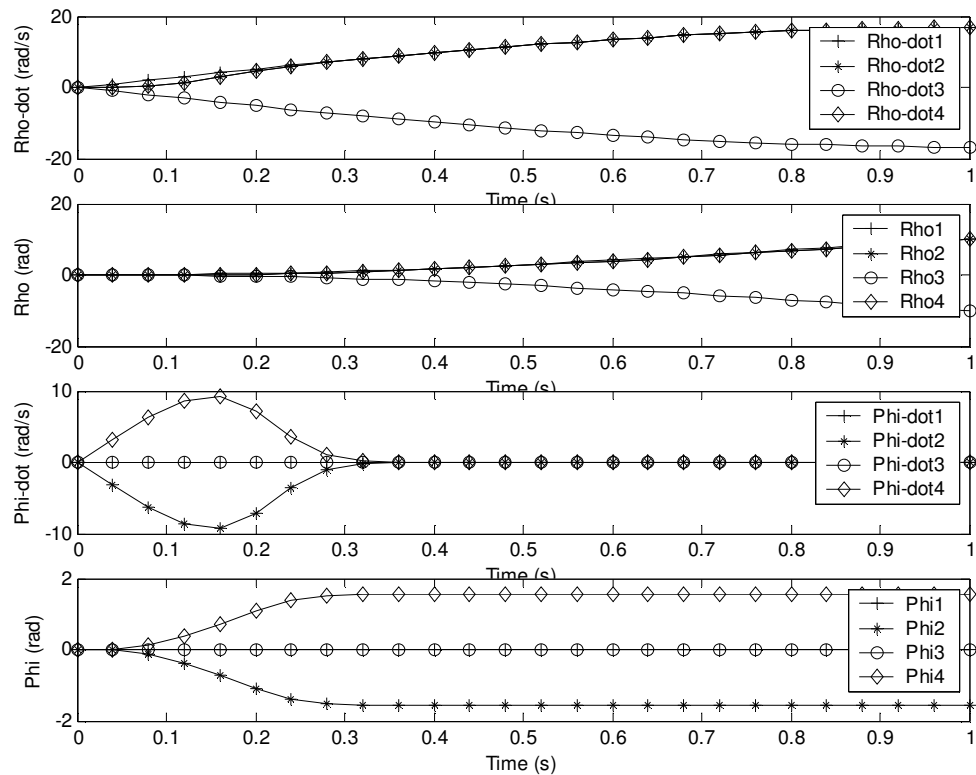


Figure 3.11: Simulation of four wheels mobile robot with applied velocity in x direction

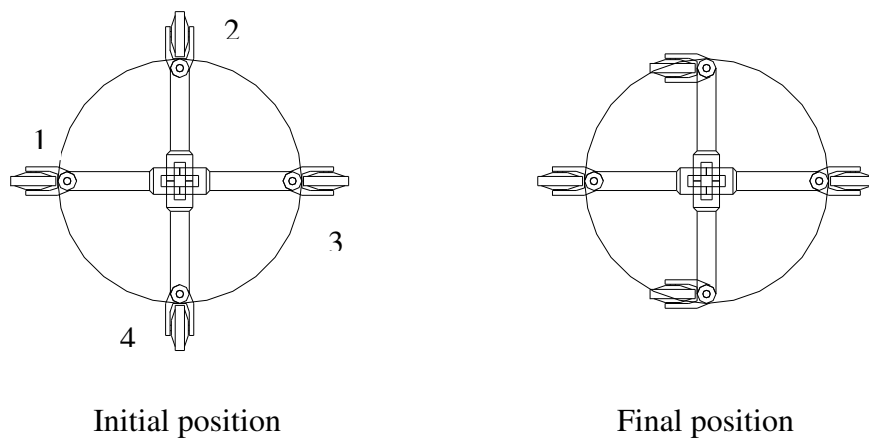


Figure 3.12: Initial and final position of four wheels mobile robot

The Figure 3.11 shows the simulation results of applying a positive velocity in the x-direction. In performing the simulation, an initial position of the mobile robot was as shown in Figure 3.12, the steering angles of all the wheels are of zero therefore all the wheels are pointing towards center of the base, which is of base frame {B}. First plot of the Figure 3.11 shows that apart from the driving velocity of the third wheel, the velocities of the other wheels are positive in magnitude as of applied velocity. If referring to the figure of final position, the steering angle of third wheel remains at zero after being applied the velocity in x direction. The reason being that is if we think of applied velocity as a force in x direction, the force in this direction will be inline with steering joint of third wheel and its contact point on the floor. This wheel, therefore, has no chance to turn as we expected. In reality, in the case of caster wheel, it should not be the case that the wheel drives with negative velocity this is however still being the correct solution obtained from the simulation. In actual implementation in the future, this will be corrected to reality means. Of particular interest to us is the turning of the wheel when the velocity is applied in x direction. As can be seen from third plot of the figure, second wheel and fourth wheel response to the applied velocity but the responses of steering velocities are different in direction. While steering velocity of fourth wheel is being positive, the velocity of second wheel is being negative. As such, the steering angles of both wheels vary as shown in forth plot until the steering velocities become zero. As expected, the steering angles of both wheels remain constant at $-\pi/2$ and $\pi/2$ respectively after vanishing of steering velocities. The initial position and final position of the four wheels mobile robot are shown in the Figure 3.12. In fact final position of the mobile robot is obtained by reading out from the plot of the simulation results.

In order to verify the correctness of our model in different direction other than x, the test velocity was applied in y direction and the results of the simulation are shown in figure below.

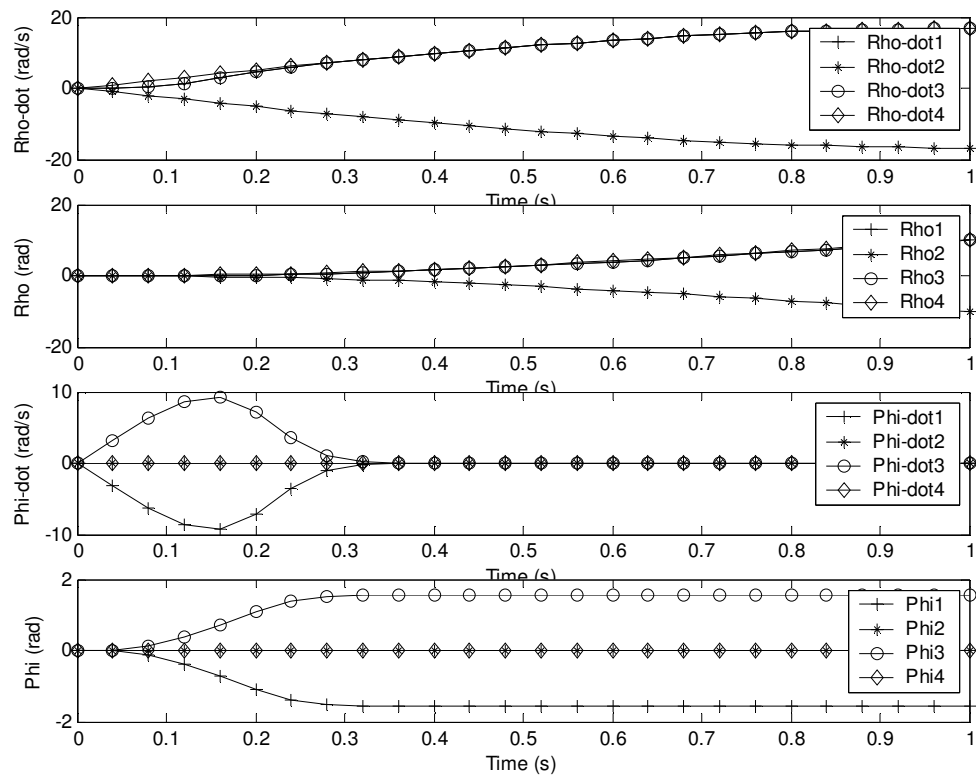


Figure 3.13: Simulation of four wheels mobile robot with applied velocity in y direction

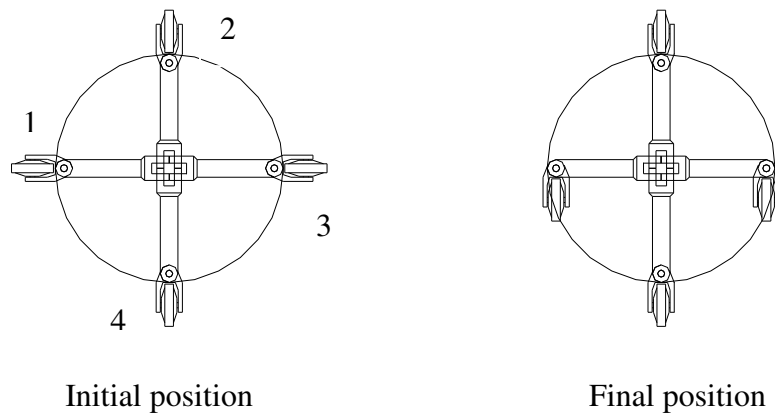


Figure 3.14: Initial and final position of four wheels mobile robot

The Figure 3.13 shows the simulation results of applying a positive velocity in the y-direction. The results of this simulation are as much the same as those of applied velocity in x direction. In performing the simulation, an initial position of the mobile robot was as shown in Figure 3.14, the steering angles of all the wheels are of zero therefore all the wheels are pointing towards center of the base, which is of base frame {B}. First plot of the Figure 3.13 shows that apart from the driving velocity of the second wheel, the velocities of the other wheels are positive in magnitude as of applied velocity. The driving angles of the wheels are shown in second plot in accordance with the driving velocities. If referring to the figure of final position, the steering angle of second wheel remains at zero after being applied the velocity in y direction. The same explanation can be applied to this situation, as was in x direction. If we think of applied velocity as a force in y direction, the force in this direction will be inline with steering joint of third wheel and its contact point on the floor. This wheel, therefore, has no chance to turn as we expected. Of particular interest to us is the turning of the wheel when the velocity is applied in y direction. As can be seen from third plot of the figure, first wheel and third wheel response to the applied velocity but the responses of steering velocities are different in direction. While steering velocity of third wheel is being positive, the velocity of first wheel is being negative. As such, the steering angles of both wheels vary as shown in forth plot until the steering velocities become zero. As expected, the steering angles of both wheels remain constant at $-\pi/2$ and $\pi/2$ respectively after vanishing of steering velocities. The initial position and final position of the four wheels mobile robot are shown in the Figure 3.14. In fact final position of the mobile robot is obtained by reading out from the plot of the simulation results.

In what follows, the results of the simulation are obtained from applying an angular velocity in counter clockwise direction on the four wheels mobile robot about z direction of its own axis.

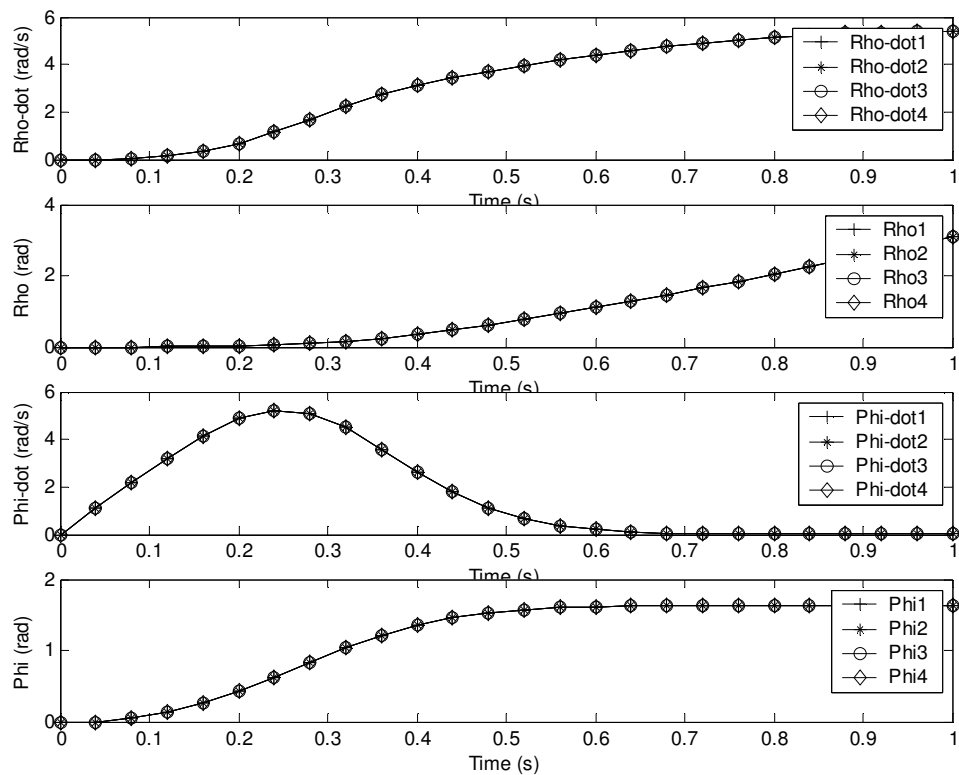


Figure 3.15: Simulation of four wheels mobile robot with applied angular velocity

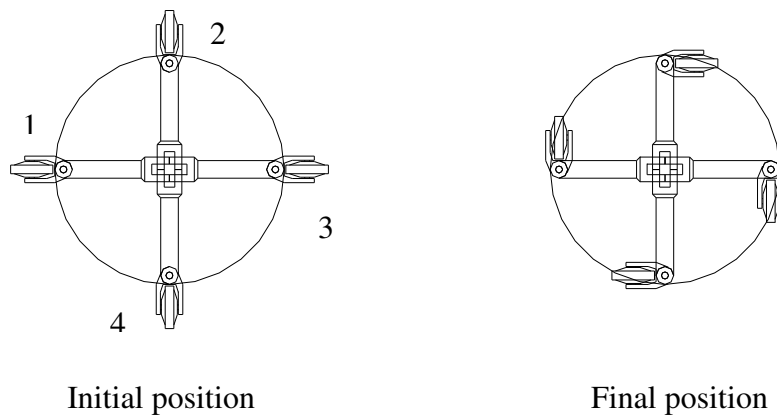


Figure 3.16: Initial and final position of four wheels mobile robot

The Figure 3.15 shows the simulation results of applying angular velocity in counter clockwise about z axis of the mobile robot. The results of this simulation are different from those of applied velocity in x and y direction. The same as preceding, in performing the simulation, initial position of the mobile robot was as shown in Figure 3.16, the steering angles of all the wheels are of zero therefore all the wheels are pointing towards center of the base, which is of base frame {B}. First plot of the Figure 3.15 shows that as we expected, driving velocities of all the wheels are the same from initial position to final position. Therefore, these velocities are in counter clockwise direction as of applied angular velocity. The driving angles of the wheels are shown in second plot in accordance with the driving velocities. Since all the driving velocities are the same so are driving angles. If referring to the figure of final position, the steering angles of all the wheels remain at $\pi/2$ after being applied the angular velocity about z direction of the mobile robot. Of particular interest to us is the steering of the wheel about the steering axis when angular velocity is applied. As can be seen from third plot of the figure, all the wheels, at the same time, response to the applied angular velocity with same magnitude and same direction about their own steering axes. As expected, the steering angles of all the wheels remain constant at $\pi/2$ after vanishing of steering velocities. The initial position and final position of the four wheels mobile robot are shown in the Figure 3.16. In fact final position of the mobile robot is obtained by reading out from the plot of the simulation results. With simulation for three different applied velocities being performed, we can conclude that these results of three simulations can provide us information about overall performance of the four wheels mobile robot under consideration.

Chapter 4

Dynamic Modeling and Analysis

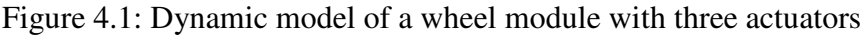
The aim of kinematic analysis is to determine the optimal design parameters that exert, as much as possible, equal effort in joint space to produce any motion in task space. In a serial manipulator, this is often reflected in a manipulability ellipsoid (Yoshikawa, 1985) at the end-effector. This is directly related to the singular issues whereby the end-effector loses the ability to move in certain direction (the degenerate direction).

In the case of a caster wheel in a mobile base system, singularity is not an issue, always not exit, as long as $r \neq 0$ and $b \neq 0$. The exception to this would be when passive joints are included in the system and only 3 joints are actuated to produce motion in 2D plane.

A manipulability ellipsoid, or more appropriately, the *maneuverability ellipsoid*, shows the velocity generated in task space with bounded joint velocities. Please note that it is not appropriate to use the Jacobian matrix in Equation 3.9, because it still reflects the contribution of the imaginary joint σ . The appropriate analysis should be performed on the J^{-1} matrix without the contribution of σ (from Equation 3.11) or the Jacobian matrix obtained from Equation 3.15.

The caster wheel is treated as a serial link manipulator, each subject to:

where τ is the torque to be sent to joint actuators, A is the inertia matrix, b is vector that contains the Coriolis and Centrifugal effects, g is the gravitational effect on the joints and q is joint coordinate. In the case of mobile robot, the gravity vector $g_i(q_i)$ is ignored since it operates only in planar motion parallel to the ground.



The matrix A of individual wheel module is derived by:

$$A = \sum_{i=1}^3 m_i J_{v_i}^T J_{v_i} + J_{\omega_i}^T I_{C_i} J_{\omega_i} \quad (4.2)$$

where the individual caster wheel is modeled as having a center of mass (m_1 , m_2 and m_3 are masses of link 1, link 2 and link 3 respectively) (see Figure 4.1), $m_i J_{v_i}^T J_{v_i}$ is kinetic energy due to the linear motion, $J_{\omega_i}^T I_{C_i} J_{\omega_i}$ is kinetic energy due to angular motion and I_{C_i} is the i^{th} link's inertia matrix evaluated at the center of mass C_i .

The Jacobian matrices J_{v1} , J_{v2} and J_{v3} are obtained by direct differentiation of the position vectors of center of mass of each link. The position vectors of center of mass of each link are obtained as:

$$P_{C1} = \begin{bmatrix} r \cos \sigma \\ r \sin \sigma \\ 0 \end{bmatrix}; P_{C2} = \begin{bmatrix} r\rho \cos \sigma \\ r\rho \sin \sigma \\ 0 \end{bmatrix} \text{ and } P_{C3} = \begin{bmatrix} r\rho \cos \sigma + 0.5h \cos(\sigma + \phi) \\ r\rho \sin \sigma + 0.5h \sin(\sigma + \phi) \\ 0 \end{bmatrix}$$

In frame $\{0\}$, the Jacobian matrices are:

$$J_{v1} = \begin{bmatrix} -rS_\sigma & 0 & 0 \\ rC_\sigma & 0 & 0 \\ 0 & 0 & 0 \end{bmatrix}; J_{v2} = \begin{bmatrix} -bS_\sigma & rC_\sigma & 0 \\ bC_\sigma & rS_\sigma & 0 \\ 0 & 0 & 0 \end{bmatrix}$$

$$J_{v3} = \frac{1}{2} \begin{bmatrix} -2bS_\sigma - hS_{\sigma+\phi} & 2rC_\sigma & -hS_{\sigma+\phi} \\ 2bC_\sigma + hC_{\sigma+\phi} & 2rS_\sigma & hC_{\sigma+\phi} \\ 0 & 0 & 0 \end{bmatrix}$$

and the Jacobian matrices $J_{\omega1}$, $J_{\omega2}$ and $J_{\omega3}$ are:

$$J_{\omega1} = J_{\omega2} = \begin{bmatrix} 0 & 0 & 0 \\ 0 & 0 & 0 \\ 1 & 0 & 0 \end{bmatrix}; \text{ and } J_{\omega3} = \begin{bmatrix} 0 & 0 & 0 \\ 0 & 0 & 0 \\ 1 & 0 & 1 \end{bmatrix}$$

The inertia tensors of masses are:

$$I_{C1} = \begin{bmatrix} I_{xx1} & 0 & 0 \\ 0 & I_{yyx1} & 0 \\ 0 & 0 & I_{zz1} \end{bmatrix}, \quad I_{C2} = \begin{bmatrix} I_{xx2} & 0 & 0 \\ 0 & I_{yyx2} & 0 \\ 0 & 0 & I_{zz2} \end{bmatrix}, \quad I_{C3} = \begin{bmatrix} I_{xx3} & 0 & 0 \\ 0 & I_{yyx3} & 0 \\ 0 & 0 & I_{zz3} \end{bmatrix}$$

Finally, the kinetic energy matrix $A(q)$ is obtained as follows:

$$A(q) = \sum_i^n m_i J_{vi}^T J_{vi} + j_{\omega i}^T I_{Ci} J_{\omega i}$$

$$A = \begin{bmatrix} A_{11} & A_{12} \\ A_{12} & A_{22} \end{bmatrix}$$

$$A_{11} = I_{zz1} + I_{zz2} + I_{zz3} + m_1 r^2 + (m_2 + m_3) b^2 + \frac{1}{4} m_3 h^2 + m_3 h b \cos \phi$$

$$A_{22} = r^2 (m_2 + m_3)$$

$$A_{33} = I_{zz3} + \frac{1}{4} m_3 h^2$$

$$A_{12} = -\frac{1}{2} m_3 r h \sin \phi$$

$$A_{13} = I_{zz3} + \frac{1}{4} m_3 h^2 + \frac{1}{2} m_3 h b \cos \phi$$

$$A_{23} = -\frac{1}{2} m_3 r h \sin \phi$$

From the partial derivatives of $A_i(q_i)$ and the generalized velocities, \dot{q}_i , the vector

$b_i(q_i, \dot{q}_i)$ can be obtained by using the Christoffel symbols. The Christoffel symbols are

$$b_{i,jk} = \frac{1}{2} (a_{ijk} + a_{ikj} - a_{jki}) \quad (4.3)$$

Using the Christoffel symbols, the centrifugal and Coriolis force vector can be written as

$$b(q, \dot{q}) = B(q)[\dot{q}\dot{q}] + C(q)[\dot{q}^2]$$

$B(q)$ and $C(q)$ matrices for our caster wheel module are obtained as:

$$B = \begin{bmatrix} 0 & -m_3hb \sin \phi & -\frac{1}{2}m_3hr \cos \phi \\ 0 & -\frac{1}{2}m_3hr \cos \phi & 0 \\ \frac{1}{2}m_3hr \cos \phi & 0 & 0 \end{bmatrix} \quad (4.4)$$

$$C = \begin{bmatrix} 0 & 0 & -\frac{1}{2}m_3hb \sin \phi \\ 0 & 0 & -\frac{1}{2}m_3hr \cos \phi \\ \frac{1}{2}m_3hb \sin \phi & 0 & 0 \end{bmatrix} \quad (4.5)$$

The operational space formulation projects the joint space dynamics of the robot into the operational space where the end-effector operates. The operational space formulation extends to the case of a mobile robot with multiple wheels. The generalized coordinates in this space are:

$$x = \begin{bmatrix} x_1 \\ x_2 \\ \vdots \\ x_N \end{bmatrix} \quad (4.6)$$

The corresponding Jacobian will be a vertical concatenation of the Jacobians for each caster wheel module:

$$J^{-1}(q) = \begin{bmatrix} J_1^{-1}(q) \\ J_2^{-1}(q) \\ \vdots \\ J_N^{-1}(q) \end{bmatrix} \quad (4.7)$$

where x_i is the position and orientation of the i^{th} end-effector, and $J_i(q)$ is the basic Jacobian which yields the velocity of i^{th} end-effector with given q . q is the vector of

generalized joint coordinates for the robot. The operational space kinetic energy matrix Λ_i is obtained for each wheel module i as:

$$\Lambda_i = ({}^B J_i A_i^{-1} {}^B J_i^T)^{-1} \quad (4.8)$$

where ${}^B J_i$ is a 3 x 3 matrix of Equation 3.3.

The combined dynamics of the mobile base at its center, expressed in Frame {B} is obtained by combining the dynamics of all the individual “serial manipulators” reflected at the end-effector (augmented object model (Khatib, 1987)):

$$\Lambda_{aug}(q) = \sum_{i=1}^N \Lambda_i(q) \quad (4.9)$$

Inertia Model

Inertia model of each link is needed to define so as to perform analysis on dynamic model. Without loss of generality, three links are modeled, respectively, as a disk with particular thickness for first link, a rectangular prism for second link, and a rectangular prism for third link, as in Figure 4.2.

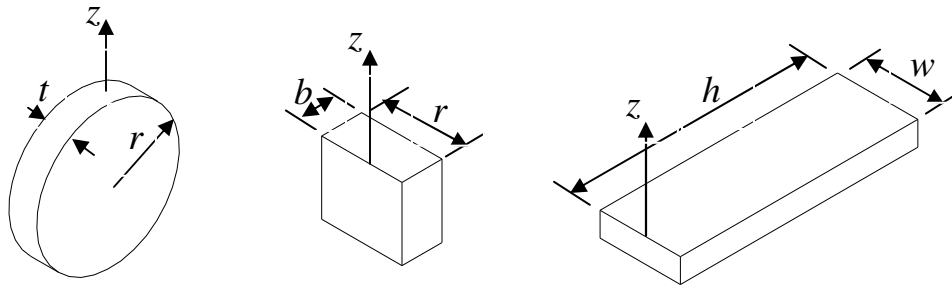


Figure 4.2: Inertia models for three links of caster wheel module

With these model defined, inertia tensor I_{zz1} , I_{zz2} and I_{zz3} in matrix A can be obtained as follows:

$$I_{zz1} = \frac{1}{12} m_1 (3r^2 + t^2) \quad (4.10)$$

$$I_{zz1} = \frac{1}{12} m_2 (4b^2 + r^2) \quad (4.11)$$

$$I_{zz1} = \frac{1}{12} m_3 (4h^2 + w^2) \quad (4.12)$$

The reader might note that the radius ‘ r ’ is being the parameter for the second link. The reason is that when the wheel radius is varied to analyze the effect on the condition number of Λ in the following section this link should physically vary in its dimension in accordance with the radius. Therefore, it should somehow relate to the wheel radius.

For analysis purpose, we define the following range of interest for all the parameters of concern so as to be of precise analysis.

Parameter	Minimum value	Maximum value
Offset b	0.01m	0.1m
Radius of wheel r	0.01m	0.1m
Thickness of wheel	0.025m	0.036m
Radius of base h	0.2m	0.4m
Mass of link 1 m1	1kg	2.6kg
Mass of link 2 m2	3kg	4.6kg
Mass of link 3 m3	10kg	50kg

Table 4.1: The ranges of the parameters of interest

Some plots in following section, we shall make use of Table 4.1 to analyze the effect of parameter variation on the performance of the mobile robot.

4.2 Dynamic Analysis

The aim of the analysis is to come up with an optimized set of design parameters so that there will be equal in producing motion in all directions. This could be done by analyzing the ellipsoid formed by the eigenvalues and eigenvectors of the Λ_{aug} matrix, which is the inertia of the mobile base in 2D task space (Asada, 1983). Since the analysis for translational and rotational motion is to be analyzed separately, it is necessary to form separate Λ matrix for translational and rotational motion:

$$\Lambda_{v_i} = ({}^B J_{v_i} A_i^{-1} {}^B J_{v_i}^T)^{-1} \quad (4.13)$$

$$\Lambda_{\omega_i} = ({}^B J_{\omega_i} A_i^{-1} {}^B J_{\omega_i}^T)^{-1} \quad (4.14)$$

where ${}^B J_{v_i}$ is the top two rows of the Jacobian matrix (for translation motion \dot{x} and \dot{y}) and

${}^B J_{\omega_i}$ is the bottom row of the Jacobian matrix for orientation ($\dot{\theta}$).

Translational Isotropy

For translational motion, the Jacobian matrix $J_{vi}(q)$ associates with the linear velocity at the operational point of each wheel module. The pseudo kinetic energy matrix at this point is:

$$\Lambda_{vi}^{-1}(q) = J_{vi}(q) A_i^{-1}(q) J_{vi}^T(q) \quad (4.15)$$

The matrix $\Lambda_{vi}^{-1}(q)$ provides a description of the end-effector of each wheel translational response to a force. To analyze the translational isotropy of single wheel, in what follows, the condition numbers of matrix $\Lambda_{vi}(q)$ is examined. In Figure 4.3, the condition number of $\Lambda_{vi}(q)$ is plotted by varying the wheel radius and offset. Moreover, to see the effect of

the steering angle on the condition number, four plots with different steering angles are presented as well.

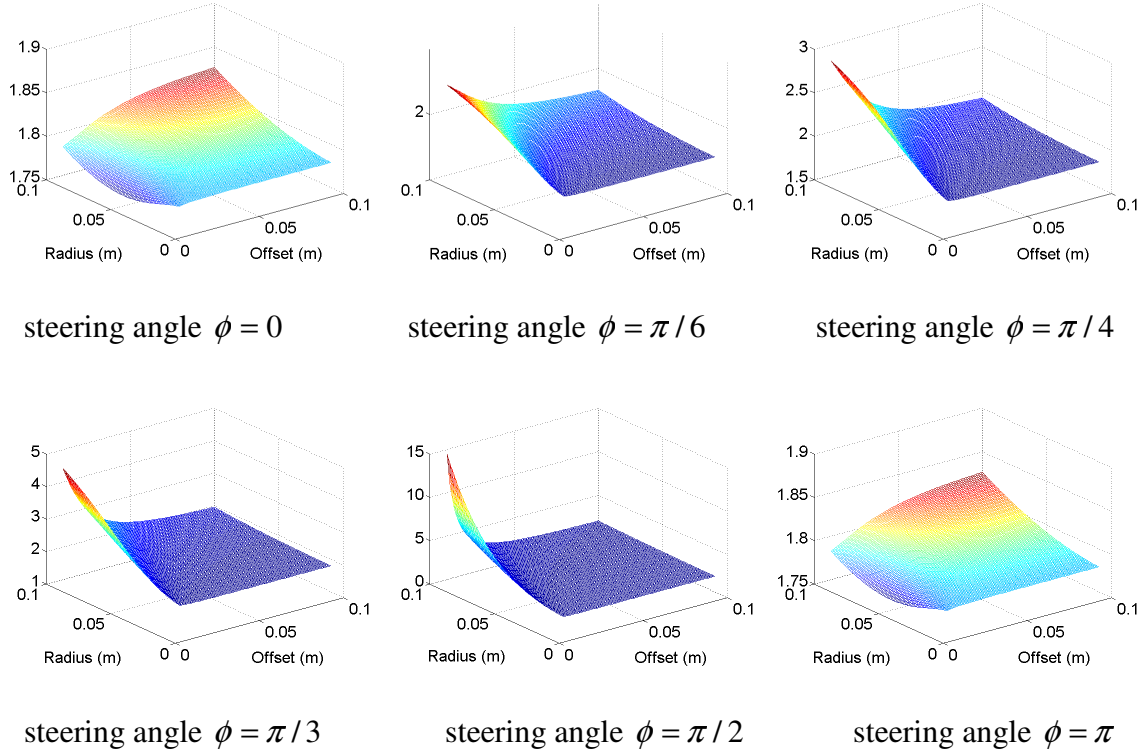


Figure 4.3: Condition number of single wheel translational pseudo kinetic energy matrix

As can be seen from the Figure 4.3, the condition number varies with offset, radius of the wheel and steering angle. Plotting in accordance with the different steering angle gives us a view of over all performance of the single wheel yet it is not the variable of our interest. In the figure, of particular interest to us is the effect of the offset on the condition number of the $\Lambda_{vi}(q)$. In all cases, the condition number is sensitive to an offset value less than 0.05m and all the condition numbers are more than 1 of isotropy condition. We thus conclude that in the case of single wheel module, it is not possible to obtain the isotropy

in the ranges of design parameters. However, the optimum value of the parameter can be chosen from the plot to give rise the best performance of the mobile robot. This figure also shows the need for the larger offset when the larger wheel is employed. It should be noted that the plot of steering angle from 0^0 to 90^0 and from 0^0 to 180^0 are the same therefore, in the follows, we shall concern the range of steering angle between from 0^0 to 90^0 .

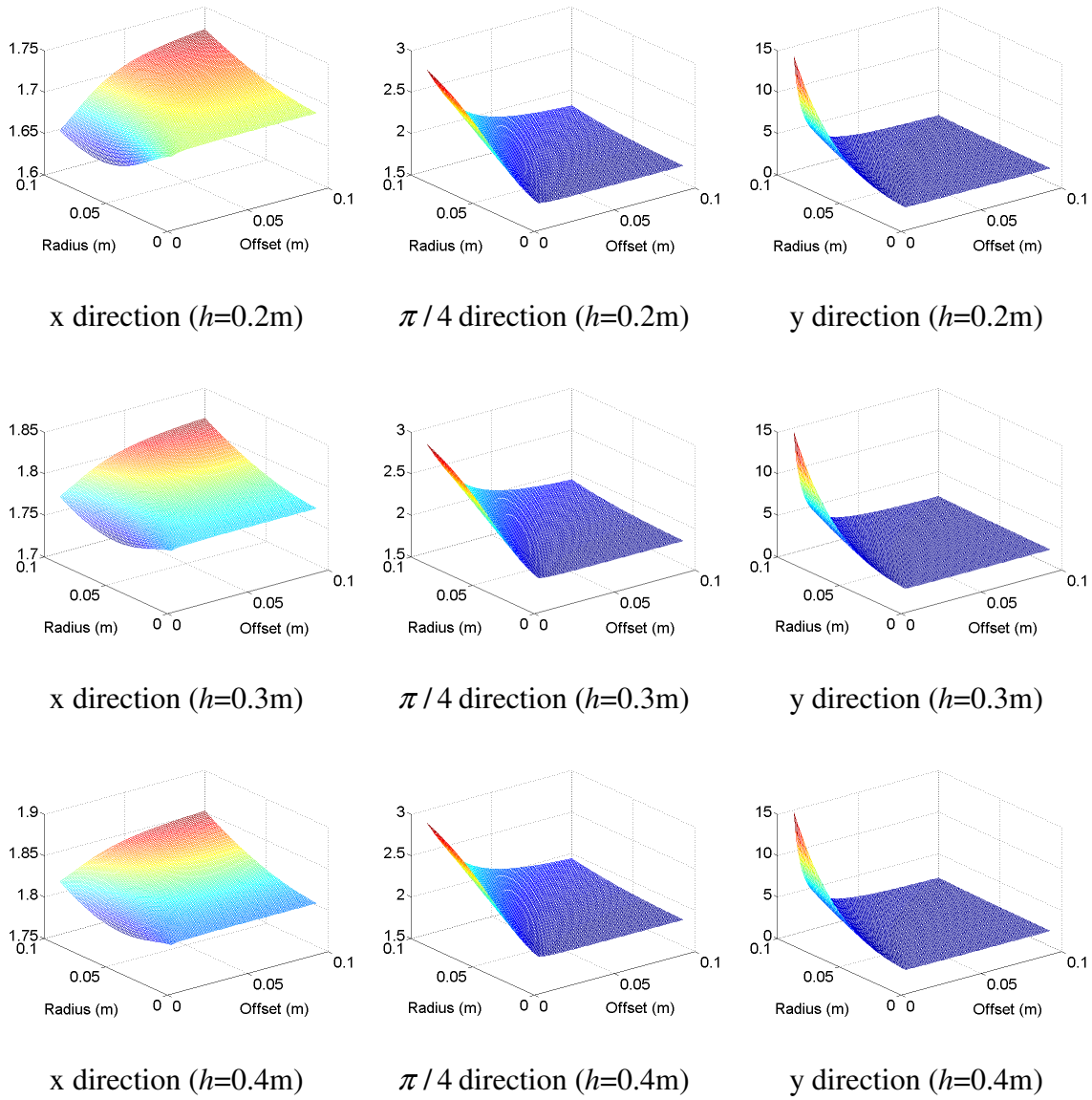


Figure 4.4: Effect of radius of the mobile base on condition number of $\Lambda_v(q)$

Figure 4.4 shows that the radius of the mobile base make not much effect on the condition number of $\Lambda_{vi}(q)$. We therefore chose the value of this parameter as for compactness of the design and leaving some allowance for the situation where mobile robot passes through doorway. With these interests we have chosen the value of 0.325m and our analysis was carried out using this value.

Rotational Isotropy

For rotational motion, the Jacobian matrix $J_{\omega}(q)$ associates with the angular velocity at the operational point of each wheel module. The pseudo kinetic energy matrix is:

$$\Lambda_{\omega}^{-1}(q) = J_{\omega}(q)A^{-1}(q)J_{\omega}^T(q) \quad (4.16)$$

The matrix $\Lambda_{\omega}^{-1}(q)$ provides a description of the end-effector of each wheel rotational response to a moment. In the case of caster wheel, the Jacobian matrix $J_{\omega}(q)$ is row vector so that the resultant pseudo kinetic matrix $\Lambda_{\omega}^{-1}(q)$ is constant rather than matrix.

$$J_{\omega} = [1 \quad 0 \quad 1] \quad (4.17)$$

From equation (4.16) and (4.17), we obtain Λ_{ω} as follows.

$$\begin{aligned} \Lambda_{\omega} = & \frac{1}{4}((I_{zz1} + I_{zz2} + m_1 r^2)m_3^2 h^2 \cos^2 \phi + (m_2^2 m_3 + m_2 m_3^2)b^2 h^2 + 8m_2 b^2 m_3 I_{zz3} \\ & + (I_{zz1} + I_{zz2} + m_1 r^2)m_2 m_3 h^2 + 4m_1 r^2(m_2 + m_3)I_{zz3} + 4(I_{zz1}m_3 + I_{zz2}m_2)I_{zz3} + \\ & 4(I_{zz2}m_3 + I_{zz1}m_2)I_{zz3} + 4(m_3^2 + m_2^2)b^2 I_{zz3})/(m_2 + m_3)((m_2 + m_3)b^2 + m_1 r^2 + I_{zz2} + I_{zz1})) \end{aligned}$$

As above, it is not possible to analysis using condition number which regards only for the matrix. We therefore leave out to analyze Λ_{ω} in the sequel.

Analysis on Multi-wheel Mobile Robot

Since single wheel module is treated as a serial manipulator, for the case of mobile robot with multi-wheel, the augmented object model (Khatib, 1987) in operational space is employed. The augmented object model provides a description of the dynamics at the operational point for a multi-manipulator system, where each manipulator has a stationary base fixed in a common inertial frame. The equation of motion of a closed-chain system under the augmented object model can be written as:

$$\Lambda_{\oplus}(x)\ddot{x} + \mu_{\oplus}(x, \dot{x}) = F_{\oplus} \quad (4.18)$$

with

$$\Lambda_{\oplus}(x) = \sum_{i=1}^N \Lambda_i(x),$$

$$\mu_{\oplus}(x, \dot{x}) = \sum_{i=1}^N \mu_i(x, \dot{x}) \text{ and}$$

$$F_{\oplus} = \sum_{i=1}^N F_i$$

where x is the operational space coordinates of the object. $\Lambda_{\oplus}(x)$, $\mu_{\oplus}(x, \dot{x})$ and $p_{\oplus}(x)$ are the operational space kinetic energy matrix, the centrifugal and Coriolis force vector, and the gravity vector associated with the manipulators. The generalized operational force vector F_{\oplus} is the resultant of the forces produced by all end-effectors at the operational point. The simplicity of the equations associated with this model is the result of an additive property that allows us to obtain the system equations of motion from the dynamics of the individual manipulators.

The translational and rotational kinetic energy matrix of augmented object can be written as:

$$\Lambda_{v\oplus}(x) = \sum_{i=1}^N \Lambda_{v_i}(x) \quad (4.19)$$

$$\Lambda_{\omega\oplus}(x) = \sum_{i=1}^N \Lambda_{\omega_i}(x) \quad (4.20)$$

Using these equations, we can perform analysis of multi-wheel by plotting the condition number of $\Lambda_{v\oplus}$. In the figure below, the condition numbers of three different mobile robots are presented.

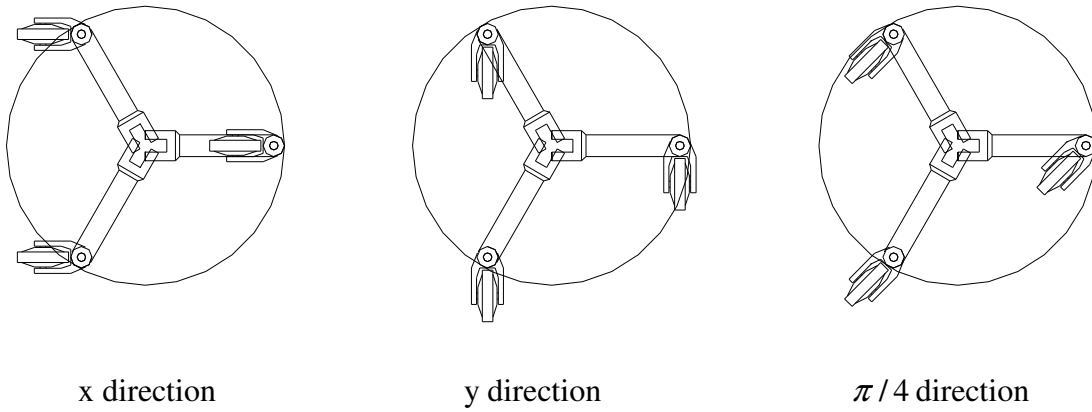


Figure 4.5: Three wheels mobile robot in three different directions

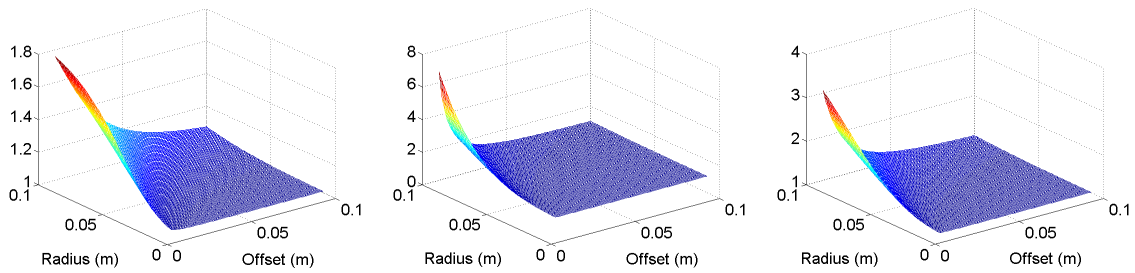


Figure 4.6: The plot of condition number of three wheels in three different directions

The plot shows that the condition number of translational kinematics energy matrix $\Lambda_{v\oplus}$ of three wheels mobile robot is small for large wheel radius and small offset in x

direction compare to those of two different directions. It seems that the condition number is very sensitive to the parameter variation but the variation of condition number is within the narrow range. In the case of two other directions, this number is sensitive to parameters within the range of offset value less than 0.04m and radius value greater than 0.05m. This plot can suggest us to choose the value of the radius and offset for optimum performance if we choose to design the mobile robot with three wheels.

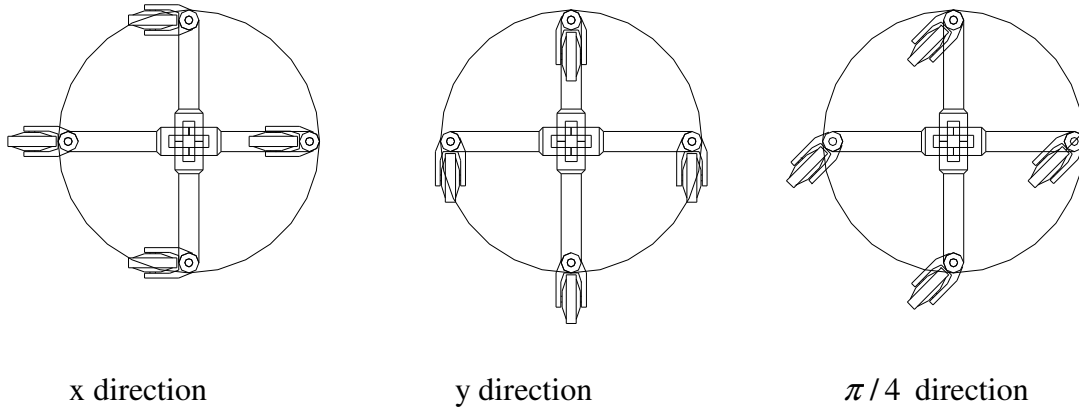


Figure 4.7: Four wheels mobile robot in three different directions

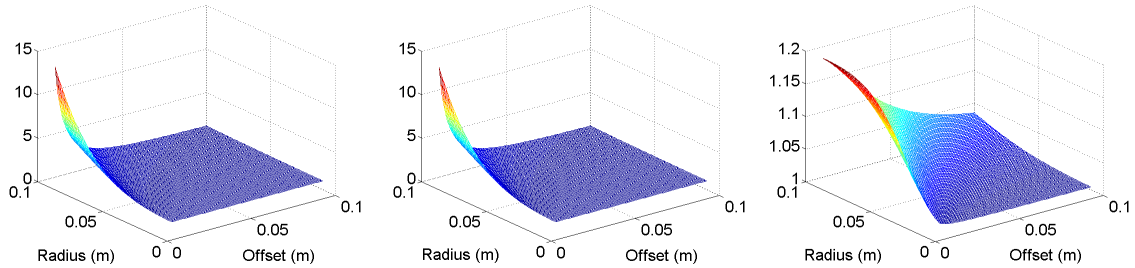


Figure 4.8: The plot of condition number of four wheels in three different directions

The plot shows that the condition number of translational kinematics energy matrix $\Lambda_{v\oplus}$ of four wheels mobile robot is small for large wheel radius (i.e., 1.2 at $r = 0.09\text{m}$) and small offset in the direction of $\pi/4$ compare to those of two different directions. It seems

that the condition number is very sensitive to the parameter variation but the variation of condition number is within the narrow range. In the case of two other directions, this number is sensitive to parameters within the range of offset value less than 0.04m and radius value greater than 0.06m. This plot can suggest us to choose the value of the radius and offset for optimum performance if we choose to design the mobile robot with four wheels.

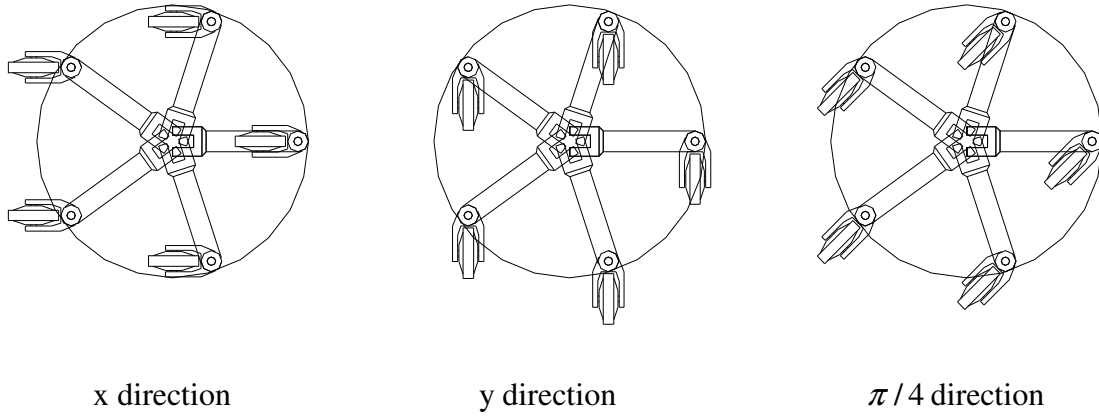


Figure 4.9: Five wheels mobile robot in three different directions

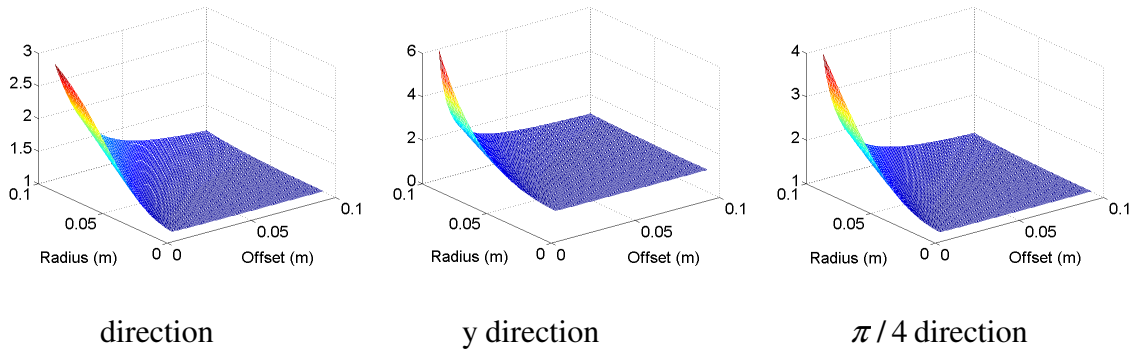


Figure 4.10: The plot of condition number of five wheels in three different directions

The plot shows that the condition number of translational kinematics energy matrix $\Lambda_{v\oplus}$ of five wheels mobile robot is small for large wheel radius and small offset in x direction

compare to those of two different directions. It seems that the condition number is very sensitive to the parameter variation but the variation of condition number is within the narrow range. In the case of two other directions, this number is sensitive to parameters within the range of offset value less than 0.04m and radius value greater than 0.05m. If compare to the plots of three wheels and four wheels, the variation of the condition number is not much in three different directions. Therefore, we can roughly conclude that five wheels configuration is the best of three in the sense that the variation of condition number is almost the same for three different directions. We will address an analysis of the effect of the number of wheel in the following section. This plot also can suggest us to choose the value of the radius and offset for optimum performance if we choose to design the mobile robot with five wheels.

Inertia Ellipsoid

As previously described, the condition number is the ratio of maximum eigenvalue to minimum eigenvalue, in particular it is best of knowing the actual value rather than ratio. In robotic literature, some researchers have proposed some analytical tools making use of these values. Asada proposed the generalized inertia ellipsoid (Asada, 1983) as a tool for the characterization of manipulator dynamics and Yoshikawa has extended the *measure of manipulability* (Yoshikawa,1985) to a *measure of dynamic manipulability* (Yoshikawa 1985).

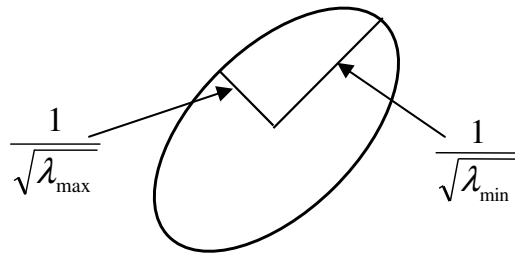
The generalized inertia ellipsoid (GIE) is to visualize the characteristic of manipulator dynamics through the geometrical representation. Associated with the generalized inertia tensor there is a quadratic surface defined by

$$x^T \Lambda x = 1 \quad (4.21)$$

Since kinetic energy is always positive, the kinetic energy matrix Λ is positive definite. Therefore the above equation is that of an ellipsoid. In the case of a single rigid body, the ellipsoid is well known as inertia ellipsoid associated with the inertia tensor I (Asada, 1983).

Basically, GIE is the extension of the inertia ellipsoid of a single rigid body to a series of rigid bodies which are of robotic manipulators. In the sequel, for the sake of simplicity, we use the term inertia ellipsoid rather than GIE.

The inertia ellipsoid has principal axes along which the inertia tensor is diagonal. The principal axes of the inertia ellipsoid are aligned with eigenvalues of the matrix Λ , and the length of each principal axis is the reciprocal of the square root of the corresponding eigenvalue. In most cases, we are interested in the motion of an end-effector mounted at the tip of the arm. Therefore the ellipsoid represents the manipulator dynamics with respect to the tip motion being referred to a cartesian coordinate system fixed in space.



where λ_{\max} and λ_{\min} are maximum and minimum eigenvalues.

Figure 4.11: Inertia ellipsoid

The principal axes of the ellipsoid are aligned with the eigenvector of Λ . The largest eigenvalue of the inertia tensor correspond to the minor axis of the inertia ellipsoid and smallest eigenvalue of the inertia tensor correspond to the major axis of the inertia ellipsoid. If the lengths of the principal axes are the same the inertia ellipsoid is a pure sphere, the resultant inertia is isotropic.

With inertia ellipsoid defined, we analyze the inertia ellipsoid of single wheel in different steering angles as in Figure 4.12.

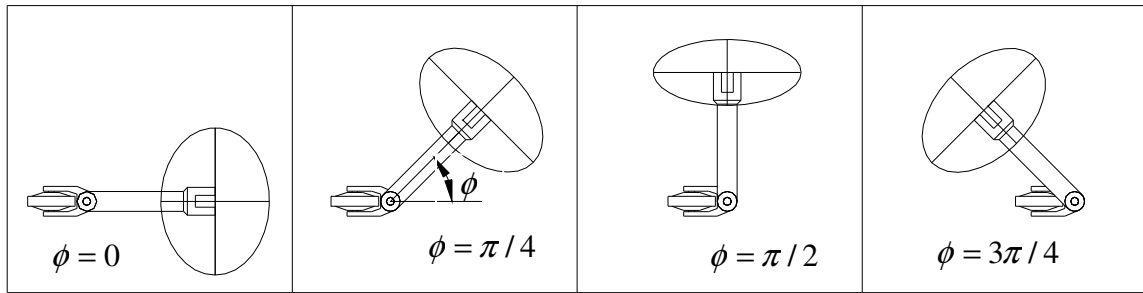


Figure 4.12: Inertia ellipsoid of single wheel in different steering angles

As can be seen in Figure 4.12, the inertia ellipsoid does not vary with the steering angle. In the case of the inertia ellipsoid at steering angle $\phi = 0$, the inertia of the wheel in x direction is larger than that of y direction, higher acceleration can therefore be produced in this direction. The same analysis applies to the wheel module in other directions. In this figure, the values used for radius of the base and the wheel, offset distance, mass of the wheel, link 2 and link 3 are 0.325m, 0.06m, 0.02m, 1kg, 3kg and 50kg respectively.

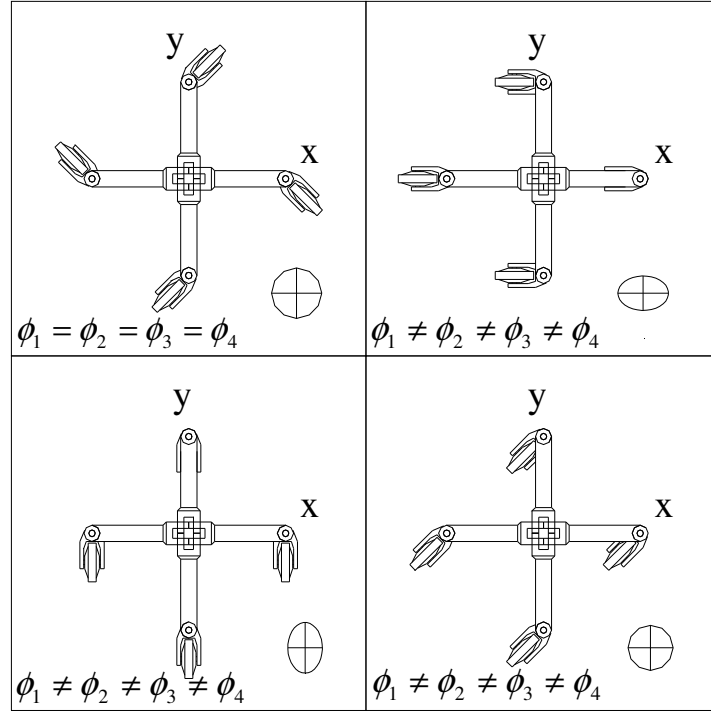


Figure 4.13: Inertia ellipsoid for translational motion of augmented mobile platform

The minor principal axis of ellipsoid shows the direction that reflects larger inertia in the motion, hence harder to move in those directions. An example of the visual representation of the reflected inertia in the 2D planar motion is shown in Figure 4.13 for translational motion for a mobile base comprised of four sets of wheel module (therefore eight actuated joints).

It is the ideal case when a mobile base is capable of moving in all directions with equal “ease”. In this case, the maneuverability ellipsoid will become a circle. Condition number of Λ can be utilized to show the ratio between the major and minor principal of the ellipsoids. The condition number of 1 means that the major and minor principal axes are of the same length.

Our dynamic analysis shows that dynamic isotropic configurations can be achieved when identical powered caster wheels (identical Λ) are distributed in polar symmetry configuration around the centre of the base. Mathematical proof can be shown by making use of the following lemmas and theorem.

Lemma 1

If $A, B = RAR^T$ (where R is rotation matrix and $A, B \in \Re^{2 \times 2}$) and $A+B$ are symmetric matrices, then

$$\lambda_k(A) + \lambda_{\min}(B) \leq \lambda_k(A+B) \leq \lambda_k(A) + \lambda_{\max}(B) \quad (4.22)$$

where k can either be *max* or *min*.

And if rotation angle of R is 0 or π , then

$$\lambda_{\max}(A+B) = 2\lambda_{\max}(A) \text{ and} \quad (4.23)$$

$$\lambda_{\min}(A+B) = 2\lambda_{\min}(A) \quad (4.24)$$

And if rotation angle of R is $\pi/2$, then

$$\lambda_{\max}(A+B) = \lambda_{\min}(A+B) = \lambda_{\max}(A) + \lambda_{\min}(A) \quad (4.25)$$

Proof. The first inequality (4.22) can be found in (Golub and Van Loan, 1989) (pp. 411), and its proof can be found in (Wilkinson, 1965) (pp. 101-2).

If $A = \begin{bmatrix} a_{11} & a_{12} \\ a_{12} & a_{22} \end{bmatrix}$ then

$$A+B = A + RAR^T$$

$$= \begin{bmatrix} a_{11} & a_{12} \\ a_{12} & a_{22} \end{bmatrix} + \begin{bmatrix} \cos \theta & -\sin \theta \\ \sin \theta & \cos \theta \end{bmatrix} \begin{bmatrix} a_{11} & a_{12} \\ a_{12} & a_{22} \end{bmatrix} \begin{bmatrix} \cos \theta & -\sin \theta \\ \sin \theta & \cos \theta \end{bmatrix}^T$$

$$= \begin{bmatrix} a_{11} + a_{22} + (a_{11} - a_{22}) \cos^2 \theta - 2a_{12} \cos \theta \sin \theta & (a_{11} - a_{22}) \sin \theta \cos \theta + 2a_{12} \cos^2 \theta \\ (a_{11} - a_{22}) \sin \theta \cos \theta + 2a_{12} \cos^2 \theta & a_{11} + a_{22} - (a_{11} - a_{22}) \cos^2 \theta + 2a_{12} \cos \theta \sin \theta \end{bmatrix}$$

if $\theta = 0$ or π then

$$A + B = 2 \begin{bmatrix} a_{11} & a_{12} \\ a_{12} & a_{22} \end{bmatrix} \text{ so } \lambda_{\max}(A + B) = 2\lambda_{\max}(A) \text{ and}$$

$$\lambda_{\min}(A + B) = 2\lambda_{\min}(A), \text{ and}$$

if $\theta = \pi/2$ then

$$A + B = \begin{bmatrix} a_{11} + a_{22} & 0 \\ 0 & a_{11} + a_{22} \end{bmatrix} \text{ and}$$

$$\lambda_{\max}(A) + \lambda_{\min}(A) = \text{trace} = a_{11} + a_{22} \quad (\text{see (Strang, 1993)})$$

therefore, $\lambda_{\max}(A + B) = \lambda_{\min}(A + B) = \lambda_{\max}(A) + \lambda_{\min}(A) \quad \square$

Example. If $B = RAR^T$,

$$A = \begin{bmatrix} 5.44 & 1.92 \\ 1.92 & 6.56 \end{bmatrix} \text{ and } R_i = \begin{bmatrix} \cos \theta_i & -\sin \theta_i \\ \sin \theta_i & \cos \theta_i \end{bmatrix} \text{ then}$$

$\lambda(A) = \{4, 8\}$, $\lambda(A + B) = \{8, 16\}$ if $\theta = 0$ and $\lambda(A + B) = \{12, 12\}$ if $\theta = \pi/2$.

Lemma 2

If $B = \sum_{i=1}^N R_i A R_i^T$ where $N \geq 3$, $A \in \Re^{2 \times 2}$ is symmetric and R is rotation matrix

with polar symmetry angle between N , then

$$\lambda_{\max}(B) = \lambda_{\min}(B) = \frac{N}{2} (\lambda_{\max}(A) + \lambda_{\min}(A)) \quad (4.26)$$

Proof. If $A = \begin{bmatrix} a_{11} & a_{12} \\ a_{12} & a_{22} \end{bmatrix}$ then

$$\begin{aligned}
 B &= \sum_{i=1}^N R_i A R_i^T \\
 &= \sum_{i=1}^N \begin{bmatrix} \cos \theta_i & -\sin \theta_i \\ \sin \theta_i & \cos \theta_i \end{bmatrix} \begin{bmatrix} a_{11} & a_{12} \\ a_{12} & a_{22} \end{bmatrix} \begin{bmatrix} \cos \theta_i & -\sin \theta_i \\ \sin \theta_i & \cos \theta_i \end{bmatrix}^T \\
 &= \sum_{i=1}^N \begin{bmatrix} a_{22} + (a_{11} - a_{22}) \cos^2 \theta_i - 2a_{12} \cos \theta_i \sin \theta_i & -a_{12} + (a_{11} - a_{22}) \sin \theta_i \cos \theta_i + 2a_{12} \cos^2 \theta_i \\ -a_{12} + (a_{11} - a_{22}) \sin \theta_i \cos \theta_i + 2a_{12} \cos^2 \theta_i & a_{11} - (a_{11} - a_{22}) \cos^2 \theta_i + 2a_{12} \cos \theta_i \sin \theta_i \end{bmatrix}
 \end{aligned}$$

if $N=3$ so $\theta = 0, \frac{2\pi}{3}, \frac{4\pi}{3}$, then

$$\begin{aligned}
 B &= \begin{bmatrix} a_{11} & a_{12} \\ a_{12} & a_{22} \end{bmatrix}_{\theta=0} + \begin{bmatrix} \frac{1}{4}a_{11} + \frac{\sqrt{3}}{2}a_{12} + \frac{3}{4}a_{22} & -\frac{\sqrt{3}}{4}a_{11} - \frac{1}{2}a_{12} + \frac{\sqrt{3}}{4}a_{22} \\ -\frac{\sqrt{3}}{4}a_{11} - \frac{1}{2}a_{12} + \frac{\sqrt{3}}{4}a_{22} & \frac{3}{4}a_{11} - \frac{\sqrt{3}}{2}a_{12} + \frac{1}{4}a_{22} \end{bmatrix}_{\theta=\frac{2\pi}{3}} \\
 &\quad + \begin{bmatrix} \frac{1}{4}a_{11} - \frac{\sqrt{3}}{2}a_{12} + \frac{3}{4}a_{22} & \frac{\sqrt{3}}{4}a_{11} - \frac{1}{2}a_{12} - \frac{\sqrt{3}}{4}a_{22} \\ \frac{\sqrt{3}}{4}a_{11} - \frac{1}{2}a_{12} - \frac{\sqrt{3}}{4}a_{22} & \frac{3}{4}a_{11} + \frac{\sqrt{3}}{2}a_{12} + \frac{1}{4}a_{22} \end{bmatrix}_{\theta=\frac{4\pi}{3}}
 \end{aligned}$$

$$B = \begin{bmatrix} \frac{3}{2}(a_{11} + a_{22}) & 0 \\ 0 & \frac{3}{2}(a_{11} + a_{22}) \end{bmatrix} \quad \text{and}$$

$$\lambda_{\max}(A) + \lambda_{\min}(A) = \text{trace} = a_{11} + a_{22} \text{ (see (Strang, 1993))}$$

$$\text{thus, } \lambda_{\max}(B) = \lambda_{\min}(B) = \frac{3}{2}(\lambda_{\max}(A) + \lambda_{\min}(A))$$

if $N=4$ so $\theta = 0, \frac{\pi}{2}, \pi, \frac{3\pi}{2}$, then

$$B = \begin{bmatrix} 2(a_{11} + a_{22}) & 0 \\ 0 & 2(a_{11} + a_{22}) \end{bmatrix} \text{ so } \lambda_{\max}(B) = \lambda_{\min}(B) = 2(\lambda_{\max}(A) + \lambda_{\min}(A))$$

if $N=5$ so $\theta = 0, \frac{2\pi}{5}, \frac{4\pi}{5}, \frac{6\pi}{5}, \frac{8\pi}{5}$, then

$$B = \begin{bmatrix} \frac{5}{2}(a_{11} + a_{22}) & 0 \\ 0 & \frac{5}{2}(a_{11} + a_{22}) \end{bmatrix} \text{ so } \lambda_{\max}(B) = \lambda_{\min}(B) = \frac{5}{2}(\lambda_{\max}(A) + \lambda_{\min}(A))$$

therefore, if $N=N$, then

$$\lambda_{\max}(B) = \lambda_{\min}(B) = \frac{N}{2}(\lambda_{\max}(A) + \lambda_{\min}(A)) \quad \square$$

Example. If $B = \sum_{i=1}^N R_i A R_i^T$

$$A = \begin{bmatrix} 5.44 & 1.92 \\ 1.92 & 6.56 \end{bmatrix} \text{ and } R_i = \begin{bmatrix} \cos \theta_i & -\sin \theta_i \\ \sin \theta_i & \cos \theta_i \end{bmatrix}$$

for $N=3$, $\theta_{1,2,3} = 0, 2\pi/3, -2\pi/3$ then $\lambda(A) = \{4, 8\}$ and $\lambda(B) = \{18, 18\}$.

By the above Lemmas and examples, it is clear that when 2 by 2 symmetric matrices are added with rotation angles between them of 90° for two and of polar symmetry for more than two respectively, then the maximum and minimum eigenvalues of the resultant matrix are the same. Using these Lemmas, we can proof the following Theorem of our interest. This Theorem will be the supplement for augmented object model in operational space (Khatib, 1987).

Theorem (Dynamically Isotropic Configuration)

If more than two planner manipulators which have two degrees of freedom are augmented with polar symmetry or two of these manipulators are augmented perpendicularly, then the configurations which are made of same corresponding angles are dynamically isotropic.

Proof:

$$\Lambda_{\oplus} = \sum_{i=1}^N R_i \Lambda_i R_i^T \quad (4.27)$$

$$= \sum_{i=1}^N R_i J_i^{-T} A J_i^{-1} R_i^T$$

Since being same corresponding angles, all the Jacobian matrices of the wheel are the same.

$$J_1 = J_2 = \dots = J_N$$

Thus, Λ_i are identical.

$$\Lambda_1 = \Lambda_2 = \dots = \Lambda_N$$

Using Lemma 1 and 2 for $N=2$ and $N \geq 3$, then

$$\begin{aligned} \lambda_{\max}(\Lambda_{\oplus}) &= \lambda_{\min}(\Lambda_{\oplus}) \\ &= \frac{N}{2} (\lambda_{\max}(\Lambda_i(x)) + \lambda_{\min}(\Lambda_i(x))). \end{aligned}$$

Therefore, Λ_{\oplus} is isotropic. \square

To get the clear picture of the Theorem, we demonstrate below by graphical mean.

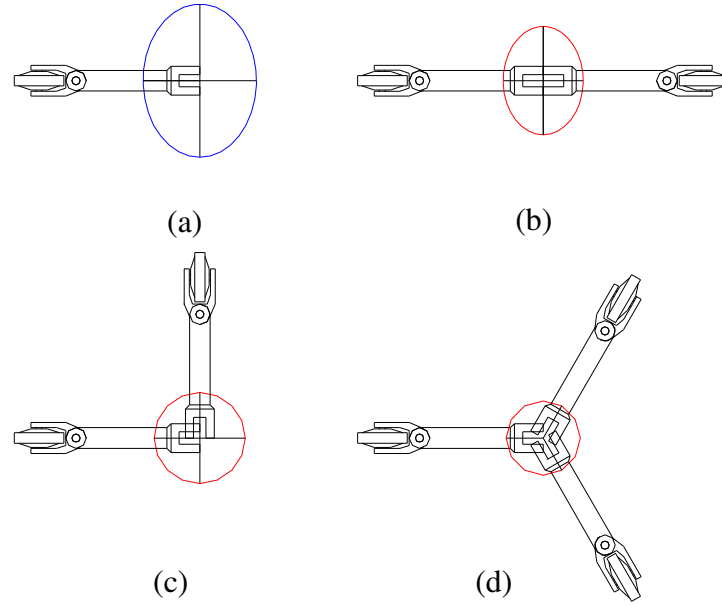


Figure 4.14: Inertia ellipsoids of the wheels in different configurations. (a) Inertial ellipsoid of single wheel. (b) Resultant ellipsoid of two wheels in 180° . (c) Resultant ellipsoid of two wheels in 90° . (d) Resultant ellipsoid of three wheels in polar symmetry. The steering angles of all the wheels are assumed to be the same.

Figure 4.14 shows that when two wheels are augmented in 180° the resultant ellipsoid is the same shape as single wheel only different in size. As we stated earlier, small in shape of the ellipsoid means that the inertia of the system becomes higher, so it reflects to physical meaning. In this figure we assume that all the steering angles of the wheels are the same so that all the Λ are identical. As theorem stated, when two wheels are augmented in 90° or more than two wheels are augmented with polar symmetry the resultant ellipsoid becomes sphere.

Analysis of Effect of Number of Wheels

In designing of the mobile robot, one of the important factors to take into consideration is the number of wheels to be used in the design. It is obvious that minimum number of wheels should be three in order to achieve the stability of the mobile robot. Of course, the higher the number of wheel, the higher the stability, however, we should take into consideration the cost of the each wheel module. If so, the question to be raised is what is the best number to be used in term of performance and the cost? To answer this question, we analyze the performance of the mobile robot with different wheel configurations in Figure 4.15.

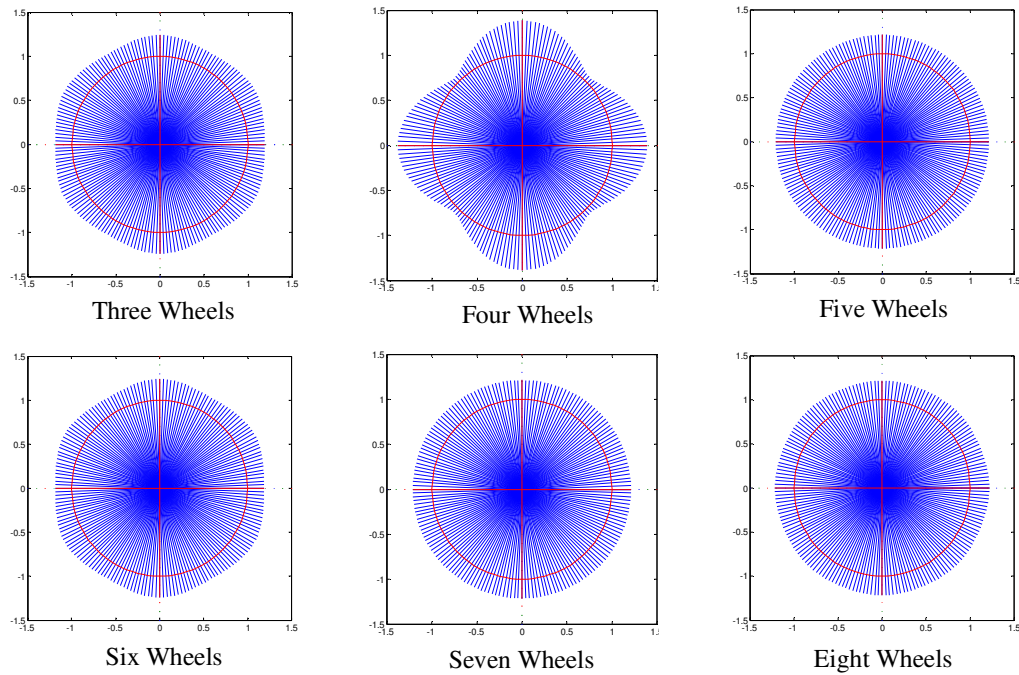


Figure 4.15: The effect of number of identical wheels on the condition number of Λ as a function of steering angle ϕ for translational motion (therefore all wheels face the same direction). The result is shown for mobile base with six different configurations distributed in polar symmetry.

Figure 4.15 shows the condition numbers of Λ in polar plot as a function of steering angle ϕ . The polar angle of each line is the steering angle ϕ and the length is the condition number of Λ . A good design would be one where condition number is close to 1 for all steering angle. The circle with radius 1, which is in red color represents the condition number of 1. From isotropy point of view, odd number wheel configurations are better than even number configurations. As can be seen in the figure, the plot for six wheels is same as three wheels, and five wheels configuration is better than six wheels and seven wheels.

Apart from the plot for the four wheels, the condition numbers for the rest of the wheel configurations are more than 1 but they are uniform in most of the configurations. Among all the configurations, the worst case scenario is four wheels configuration. The reason being that is when four wheels mobile robot moves in x-direction the shape of an ellipsoid of the wheel with steering angle 0° and the shape of an ellipsoid of the wheel with steering angle 180° are the same. When these same shape ellipsoids are added together the shape of resultant ellipsoid is same as two ellipsoids but different in size.

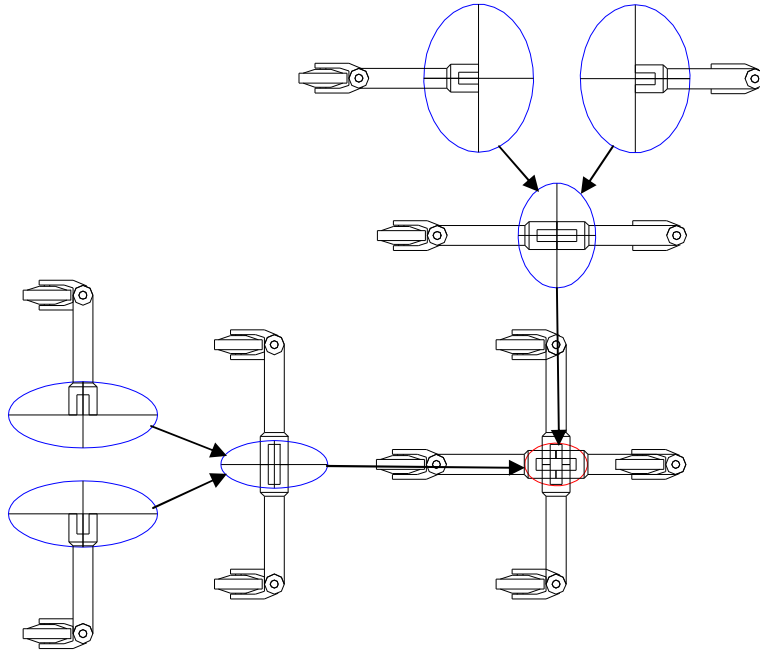


Figure 4.16: Augmentation of ellipsoid in four wheels mobile robot

Of particular interest to us is four wheels configuration since its CNPP is different from others.

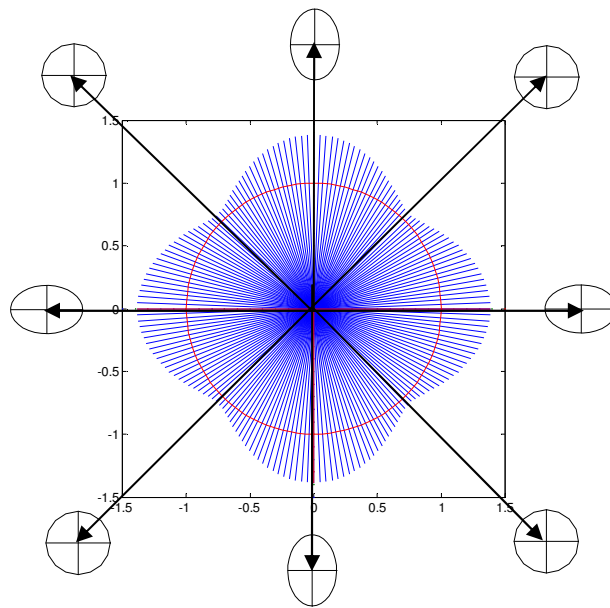


Figure 4.17: CNPP of four wheels

The Figure 4.17 shows dependency of the condition number on steering angle, with five wheels configuration showing least dependency. It is interesting to note that the four wheel configuration achieves condition number of 1 only at $\pm 45^\circ$, and $\pm 135^\circ$ therefore the inertias ellipsoid are in circle shapes. At 0° , 90° , 180° and 270° the magnitudes of the condition numbers are more than isotropic number 1 so that the shapes of inertias become ellipses. This plot could be used as a tool for designing a mobile base to achieve isotropic effect with different design parameters.

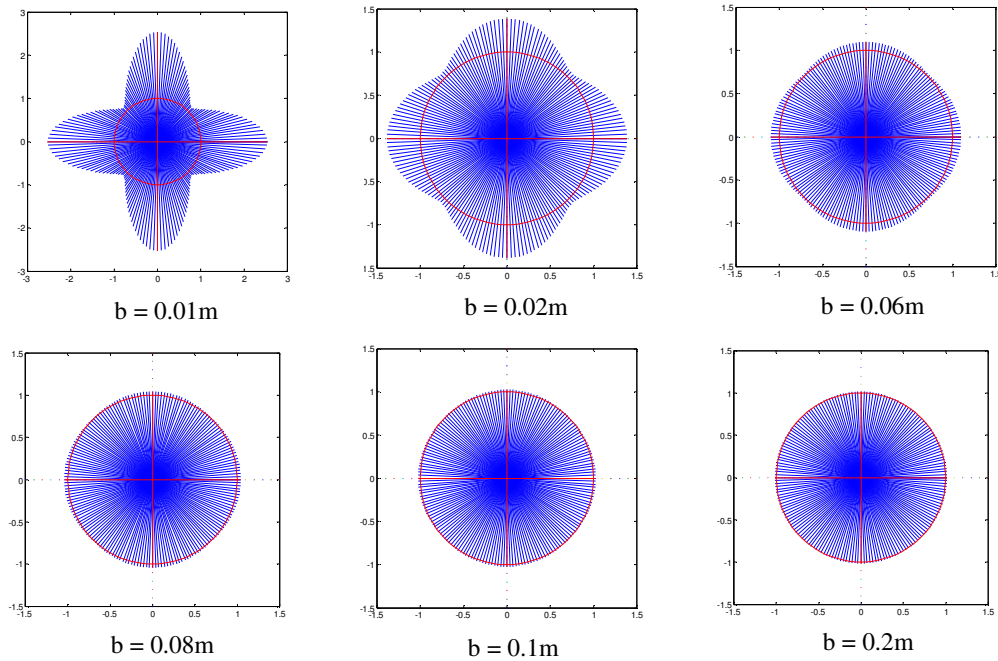


Figure 4.18: Effect of offset b on four wheels mobile robots

As we described, Figure 4.18 shows that the length of offset b largely effects the isotropy of the mobile robot. In particular, offset b of 0.06m can grantee better performance than that of smaller one. However, on the other hand, when offset is increased the require torque to drive the steering joint is also increase accordingly. Therefore, if we can

sacrifice a little improvement in performance we shall achieve smaller torque to drive the steering joint.

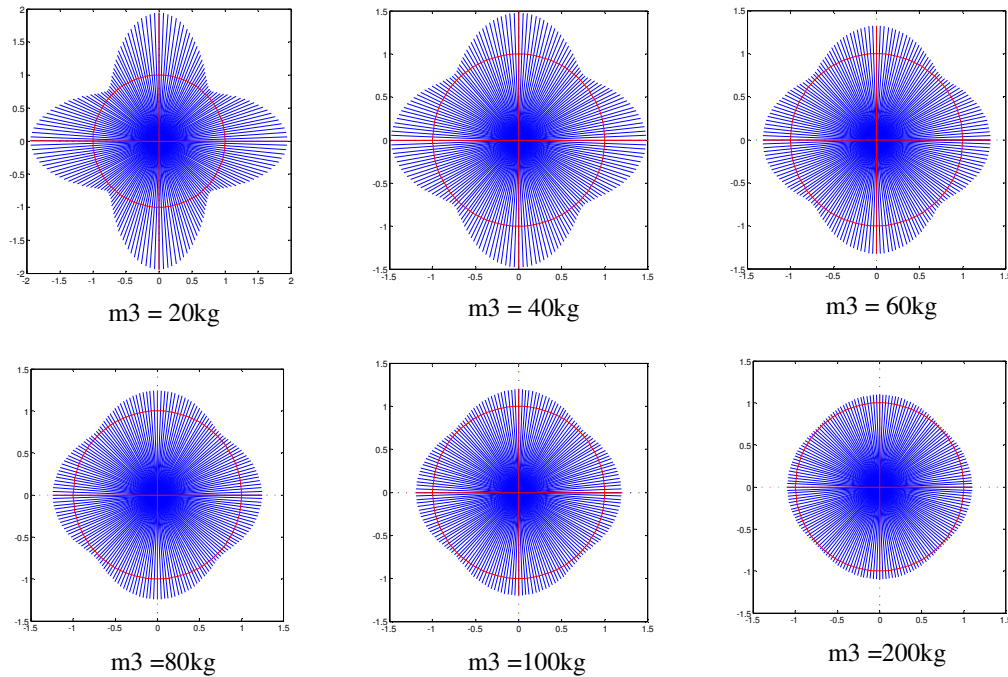


Figure 4.19: Effect of mass of link three on four wheel mobile robot

As can be seen in Figure 4.19, with heavier mass of the link three, we can achieve isotropy of the mobile robot. However, if the mass is heavy the require torque to drive this link will be higher than that of lighter one, as was in offset.

Dynamic Isotropy and Singularity

Another interesting to take note is that our CNPP plots represent not only isotropy but also singularity of the system. As we described in previous section, the condition number is the ratio of maximum singular value to minimum singular value so that when minimum singular value becomes zero the condition number is infinity. Therefore, the length of the

line representing this condition number will be very long in our plots. As an example, two links manipulator is used.

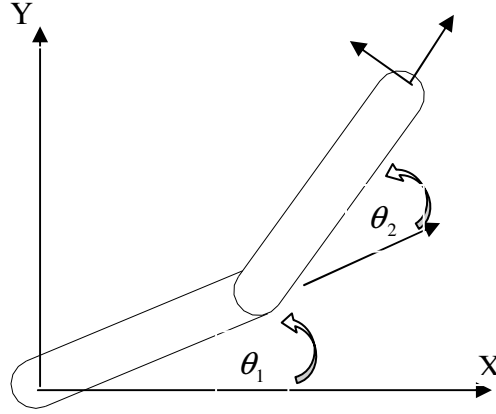


Figure 4.20: Two links manipulator

The Jacobian matrix and inertia matrix of the two links manipulator can be easily found in (Craig, 1989).

$$A = \begin{bmatrix} m_1 l_1^2 + I_{zz1} + m_2 l_1^2 + 2m_2 l_1 l_2 \cos \theta_2 + m_2 l_2^2 + I_{zz2} & m_2 l_1 l_2 \cos \theta_2 + m_2 l_2^2 + I_{zz2} \\ m_2 l_1 l_2 \cos \theta_2 + m_2 l_2^2 + I_{zz2} & m_2 l_2^2 + I_{zz2} \end{bmatrix} \quad (4.28)$$

$$J_v = \begin{bmatrix} -l_1 \sin \theta_1 - l_2 \sin(\theta_1 + \theta_2) & -l_2 \sin(\theta_1 + \theta_2) \\ l_1 \cos \theta_1 + l_2 \cos(\theta_1 + \theta_2) & l_2 \cos(\theta_1 + \theta_2) \end{bmatrix} \quad (4.29)$$

$$J_\omega = [1 \quad 1]$$

Using (4.28) and (4.29), the translational pseudo kinetic energy matrix is obtained as:

$$\Lambda_v = (J_v A^{-1} J_v^T)^{-1} \quad (4.30)$$

In plotting the condition number of translational pseudo kinetic energy matrix (4.30) of two links manipulator, we fixed the angle of first link at 0° and then the angle of link 2 is varied. The resulting plot is shown in Figure 4.21.

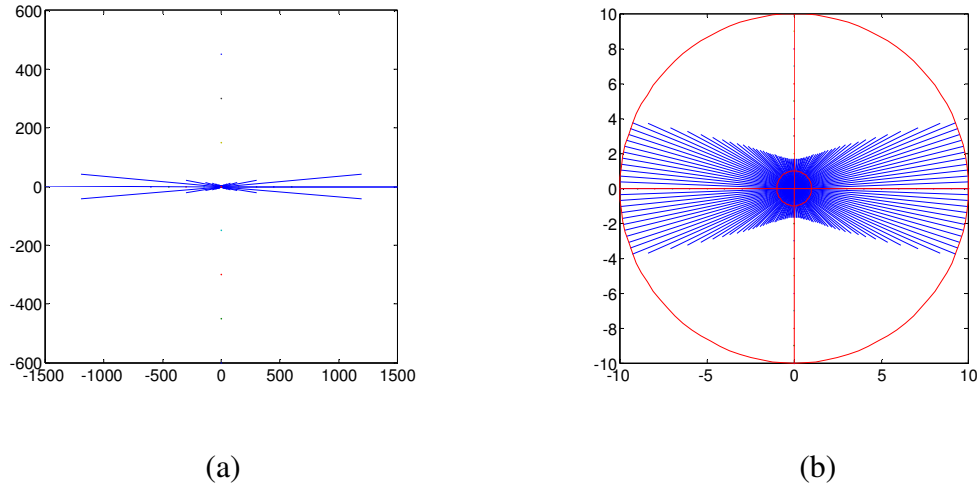


Figure 4.21: (a) CNPP of two links manipulator
(b) Close up view of isotropy and singular region

As can be seen from Figure 4.21(a), the inertia matrix is singular at 0° and at 180° of second link therefore the condition number is very large at these angles. For simplicity and for clarity, we limited the condition number at singularity region to be of 10 in figure (b) as close up view. Therefore, in the figure, the outer circle represents the singularity while inner unit circle represents the isotropy of the manipulator. It is obvious that, for ideal case, if the isotropy is achieved then there would be no singularity.

The Design of Caster Wheel

We have designed the caster wheel module using the offset value of 0.02m and total payload of 25kg. The detail computation for motor sizing can be found in Appendix A and the detail drawing can be found in Appendix B.

Chapter 5

Conclusions

5.1 Summary

In this thesis, we have presented the kinematic of one class of omni-directional mobile robots, whose designs are motivated by 2-axis powered caster wheels with non-intersecting axes of motion. Complete kinematic of the wheel and the base are completely derived using Denavit-Hartenberg parameterization. Our approach treats the caster wheel as a serial robot and is physically intuitive. As expected, our derived kinematic model is exactly the same as that of (Muir, 1988) which involves extensive computation of matrix transformation.

The kinematic analysis is carried out by analyzing the condition number of Jacobian matrix. It was found that an optimal length of offset and radius of the wheel are essential so that motion in all direction can be produced with equal effort. Furthermore, our analysis shown that the kinematic performance of mobile robot is less dependency on steering angle, radius of the mobile robot and number of wheels.

The dynamic of single wheel is derived from the serial robot model and multi-wheel mobile robot is derived using the operational space approach and augmented object

model introduced by (Khatib, 1987). We have described two lemmas to proof the theorem of “Dynamically Isotropic Configuration” as a supplementary tool for augmented object model in operational space. Our dynamic analysis shows that dynamic isotropic configurations can be achieved when more than two identical caster wheels (identical Λ) are distributed in polar symmetric or in 90° , in the case of two wheels, configuration around the center of the base. Mathematical proof is shown by making use of two lemmas and theorem.

The dynamic analysis is carried out by analyzing the condition number of operational space pseudo kinetic energy matrix, and further analysis is carried out by utilizing the *Generalized Inertia Ellipsoid*. The results of dynamic analysis agree with that of kinematic.

5.2 Recommendation for Future Work

In chapter 3, we presented the kinematic analysis of single wheel by utilizing the manipulability ellipsoid introduced by (Yoshikawa, 1985). In the case of multi-wheel, it is not possible to utilize this approach due to kinematic constraints. For this reason we have left out to analyze the mobile robot with multi wheel. More work need to be done on this issue.

In deriving the kinematic model, we did not take into account the effect of wheel slippage. To get better accuracy in kinematic performance, some uncertainties such as wheel elasticity, friction, etc., should be taken into consideration. Furthermore, some analysis should be done on characteristics of wheels to be used in design, since the shapes

of the wheel determine the force distributions in contact area at contact patch between wheel and ground. The shape of the wheel can also affect the accuracy of performance of mobile manipulation.

In analysis of mobile robot, we have left out to address the stability issue, since our mobile robot is designed to maneuver in slow speed. However, in the case of high speed mobile manipulation, this issue will be crucial for its performance.

References

- Alexander, J. C. and Maddocks, J. H., 1989, May, "On the Kinematics of Wheeled Mobile Robots," *International Journal of Robotics Research*, Vol. 8, No. 5, pp. 15-27.
- Angeles, J., Ranjbaran, F. and Patel, R. V., 1992a, "On the Design of the Kinematics Structure of Seven-axes Redundant Manipulators for Maximum Conditioning," *Proceedings IEEE International Conference on Robotics and Automation*, Nice, France, pp. 494-499,
- Angles, J., 1992b, "The Design of Isotropic Manipulator Architectures in the Presence of Redundancies," *International Journal of Robotics Research*, Vol. 11, No. 3, pp. 196-201.
- Asada, H., 1983, "A Geometrical Representation of Manipulator Dynamics and Its Application to Arm Design," *Transactions ASME, Journal of Dynamic System Measurement and Control*, Vol. 105, pp. 131-135.
- Asada, H. and Slotine, J. J. E., 1986, "Robot Analysis and Control," John Wiley and Sons.

- Bastin, G. and Campion, G., 1989, "On Adaptive Linearization Control of Omnidirectional Mobile Robots," *Proceedings of MTNS 89, Progress in Systems and Control Theory* 4, Amsterdam, Vol. 2, pp. 531-538.
- Campion, G., Bastin, G. and D'Andrea-novel, B., 1996, February, "Structural Properties and Classification of Kinematics and Dynamic Models of Wheeled Mobile Robots," *IEEE Transactions on Robotics and Automation*, Vol. 12, pp. 47-62.
- Cheng, R. M. H. and Rajagopalan, R., 1992, "Kinematics of Automated Guided Vehicles with an Inclined Steering Column and an Offset Distance-Criterion for Existence of Inverse kinematics colution," *Journal of Robotics System.*, 9(8), 1059-1081.
- Craig, J. J., 1989, "Introduction to Robotics: Mechanics and Control," 2nd ed., Addison-Wesley, Reading, MA.
- D'Andrea-Novels, B., Bastin, B. and Campion, G., 1991, "Modeling and Control of Nonholonomic Wheeled Mobile Robots," *Proceedings of IEEE Confrence on Robotics and Automation*, Sacramento, CA, pp.1130-1135.
- Denavit, J., and Hartenberg, R. S., 1955, "A Kinematic Notation for Lower-Pair Mechanisms Based on Matrices," *Journal of Applied Mechanics.*, vol 77, pp 215-221.

- Desa, S. and Kim, Y., 1990, "Definition, Determination, and Characterization of Acceleration Sets for planar manipulators," *Flexible Mechanism, Dynamics, and Robot Trajectories*, DE v.24, ASME, New York, NY, pp. 207-215.
- Ferriere, L. Raucourt, B. and Campion, G., 1996, "Design of Omnidirectional Robot Wheels," *Proceedings of International Conference on Robotics and Automation*, Vol.4, pp.3664-3670.
- Ferriere, L. Raucourt, B. and Fournier, A., 1996, "Design of a Mobile Robot Equipped with Off-centered Orientable Wheels", *Proceedings of the Research Workshop of ERNET*, pp. 127-136.
- Fu, K. S. Gonzalez, R. C. and Lee, C. S. G., 1987, "Robotics: Control, Sensing, Vision, and Intelligence," McGraw-Hill International Editions, Industrial Engineering Series.
- Goldstein, H., 1950, "Classical Mechanics", Addison-Wesley.
- Golub, G. and Van Loan, C., 1989, "Matrix Computations." Johns-Hopkins, Baltimore, second edition.

Graettinger, T. J. and Krogh, B., 1988, February, "The Acceleration Radius: A Global Performance Measure for Robotic Manipulators," *IEEE Journal of Robotics and Automation*, Vol 4, No. 1, pp. 60-69.

Holmberg, R., 2000, August, "Design and Development of Powered-caster Holonomic Mobile Robots," PhD. Dissertation, Stanford University.

Khatib, O., 1987, "A Unified Approach for Motion and Force Control of Robot Manipulators: The Operational Space Formulation," *IEEE Journal of Robotics and Automation*, Vol. RA-3, No. 1, pp. 43-53.

Khatib, O and Burdick, J., 1987, "Optimization of Dynamics in Manipulator Design: The Operational Space Formulation," *International Journal of Robotic and Automation*, Vol 2, No. 2, pp90-98.

Killough, S. M. and Pin, F. G., 1992, May, "Design of an Omnidirectional and Holonomic Wheeled Platform Prototype", *Proceedings of IEEE International Conference on Robotics and Automation*, Nice, France.

Kircanski, M. V., 1994, "Robotic Isotropy and Optimal Design of Planar Manipulators," *Proceedings of IEEE International Conference on Robotics and Automation*, San Diego, USA, pp. 1100-1105.

- Klein, C. A. and Blaho, B. E., 1987, "Dexterity Measure for the Design and Control of Kinematically redundant manipulators," *International Journal of Robotics Research*, Vol. 6, No. 2, pp. 72-83.
- La, W., Koogle, T., Jaffe, D. L. and Leifer, L., 1981, "Toward Total Mobility: An Omnidirectional Wheelchair," *Proceeding of 4th RESNA*, pp. 75-77.
- Ma, O. and Angeles, J., 1990, May, "The Concept of Dynamic Isotropy and Its Application to Inverse Kinematics and Trajectory Planning", *Proceedings of 1990 IEEE International Conference on Robotics and Automation.*, Cincinnati, pp. 481-486.
- Muir, P. F. and Numan, C. P., 1987a, "Kinematic Modeling of Wheeled Mobile Robots," *Journal of Robotics Systems*, Vol. 4, No. 2, pp.281-340.
- Muir, P. F. and Numan, C. P., 1987b, "Kinematic Modeling for Feedback Control of an Omnidirectional Wheeled Mobile Robot," *Proceedings IEEE International Conference on Robotics and Automation*, pp 1772-1778.
- Muir, P. F. and Numan, C. P., 1987c, "Kinematic Modeling of Wheeled Mobile Robots," *Journal of Robotic System*. Vol. 4, No 2, pp. 281-329.

Muir, P. F., 1988, August, "Modeling and Control of Wheeled Mobile Robots," Ph.D. Thesis, Carnegie Mellon University.

Ostrovskaya, S., Angeles, J. and Spiteri, R., 1998, "Nonholonomic Systems Revisited within the Framework of Analytical Mechanisms," *Applied Mechanics Review*, Vol. 51, No. 7, pp 415-433.

Ostrovskaya, S., Angeles, J. and Spiteri, R., 2000, "Dynamics of a Mobile Robot with Three Ball-wheels," *The International Journal of Robotics Research*, Vol. 19, No.3, pp.1-11.

Paromtchik, I. and Rembold, U., 1994, "Practical Approach to Motion Generation and Control for an Omnidirectional Mobile Robot," *Proceedings of IEEE International Conference on Robotics and Automation*, vol. 4, pp. 2790-2795.

Paul, R. P., 1981, "Robot Manipulators, Mathematics, Programming and Control," MIT Press, Cambridge, 1981.

Paul, R. P. and Stevenson, C. N., 1983, "Kinematics of Robot Wrists," *The International Journal of Robotics Research*, Vol. 2, No. 1, pp. 31-38.

- Pin, F. G. and Killough, S. M., 1994, August, "A New Family of Omnidirectional and Holonomic Wheeled Platforms for Mobile Robots", *IEEE Transactions on Robotics and Automation*, Vol. 10, No.4, pp 480-489.
- Saha, S. K. and Angeles, J., 1989, "Kinematics and Dynamics of a Three-wheeled 2-DOF AGV," *Proceedings of IEEE International Conference on Robotics and Automation*, Scottsdale, AZ, pp. 1572-1577.
- Salisbury, J. K. and Craig, J. J., 1982, "Articulated Hands: Force Control and Kinematics issues," *International Journal of Robotics Research*, Vol. 1, No. 1, pp. 4-17.
- Sciavicco, L. and Siciliano, B., 1996, "Modeling and Control of Robot Manipulators," McGraw-Hill Co., Inc.
- Sheth, P. N. and Uicker, J. J., 1971, February, "A generalized symbolic notation for mechanisms," *Journal of Engineering for Industry*, Series B, Vol.93, No.70-mech19, pp102-112.
- Strang, G., 1993, "Introduction to Linear Algebra", Wellesley, MA: Wellesley-Cambridge Press.
- Wada, Wada., Tominaga, Y., and Mori, S., 1995, August, "Omnidirectional holonomic mobile robot using nonholonomic wheels," *Proceeding IEEE/RSJ International*

Conference on Intelligent Robots and Systems, Vol 3, pp 446 -453.

Wada, M. and Mori, S., 1996, "Holonomic and Omnidirectional Vehicle with Conventional Tires," *Proceedings of IEEE International Conference on Robotics and Automation*, Vol. 1, pp. 265-270.

West, M. and Asada, H., 1995, "Design and Control of Ball wheel Omnidirectional Vehicles," *Proceedings IEEE International Conference on Robotics and Automation*, Nagoya, Japan, Vol. 2, pp. 1931-1938.

West, M. and Asada, H., 1997, "Design of Ball Wheel Mechanisms for Omnidirectional Vehicles with Full mobility and invariant kinematics," *Journal of Mechanical Design*, Vol. 119, pp153-161.

Wilkinson, J. H., 1965, "The Algebraic Eigenvalue Problem," Clarendon Press, Oxford.

Williams, D. and Khatib, O., 1993, "The Virtual Linkage: A Model for Internal Forces in Multi-grasp Manipulation," *Proceedings of IEEE International Conference on Robotics and Automation*, Vol. 3, pp. 1025-1030.

Yi, B. J. and Kin, W. K., 2002, "The Kinematics for Redundantly Actuated Omnidirectional Mobile Robots," *Journal of Robotic Systems*, Vol. 19, No. 6, pp. 255-267.

Yoshikawa, T., 1985, Summer, "Manipulability of Robotic Mechanisms, " *International Journal of Robotics Research*, Vol. 4, pp. 3-9.

Zaw, M. T., Denny, O., Marcelo, H. A. J. and Ng, T. K., 2003a, "Kinematics and Dynamics of an Omnidirectional Mobile Platform with Powered Caster Wheels", *International Symposium on Dynamics and Control*, Hanoi.

Zaw, M. T., Denny, O., Marcelo, H. A. J., Lim, C. W. and Ng, T. K., 2003b, "Modeling and Analysis of Omnidirectional Mobile Robot Toward Isotropic Design", *International Conference & Exhibition on Instrumentation and Control*, Manila.

Appendix A

Design of Powered Caster Wheel Module

In our caster wheel design, two motors are utilized. One motor is for steering and another one is for deriving. The conventional off-the-shelf solid rubber tire is utilized and is chosen to sustain the weight of 150kg. In deriving mechanism, the spur gears are used to reduce the speed of the motor, and the power is transmitted through the center of worm gear to bevel gear which is attached to the wheel. On the other hand, by reducing the speed of motor, torque of the output is increased accordingly. The gear ratios in this mechanism are 4:1 and 3:1 for spur gear and bevel gear, respectively, therefore total gear ratio is of 12:1.

In steering mechanism, to achieve not only high accuracy but also to reduce the speed, the worm gear and bevel gear are used so that the power is transferred through the bevel gear to worm gear which is attached to the steering wheel mechanism. The gear ratios in this mechanism are 1.5:1 and 50:1 for bevel gear and worm gear, respectively, therefore the total gear ratio is of 75:1.

A.1 Computation for Rolling Torque

In this section, we make use of the methodologies from the literature of ground vehicle which have been established for many decades.

The rolling resistance of the caster wheel is computed based on the total payload of the mobile robot. The load of 100kg is assumed to be the total payload therefore in the case of mobile robot with four wheels each wheel has to carry the weight of 25kg. In general, the rolling resistance is varied with the type of floor surface and weight of the load on the wheel. In our computation, the value of 0.08 is used for coefficient of rolling resistance. The computation of rolling resistance is as follows:

$$F_{rolling} = C_r W \quad (A.1)$$

$$= 0.08 \times 100 \times 9.8 = 78.4\text{N}$$

$$T_{rolling} = F_{rolling} r \quad (A.2)$$

$$= 78.4 \times 0.0625 = 4.9\text{N-m}$$

where $W = mg$

$F_{rolling}$ = rolling resistance

C_r = rolling resistance coefficient

W = weight

$T_{rolling}$ = rolling resistance torque

r = radius of wheel

A.2 Computation for steering torque

In finding the required torque to steer the wheel, we utilize the friction force that prevents slipping. It relates to the normal force N acting on the wheel and the frictional coefficient, μ . The coefficient of friction, μ , is a characteristic of the wheel and the floor material.

For a rubber wheel and a concrete floor, μ is about 0.8. The computation of fraction force is as follows:

$$F_{steering} = \mu N \quad (A.3)$$

$$= 0.8 \times 100 \times 9.8 = 784 \text{ N}$$

$$T_{steering} = F_{steering} d_{swivel} \quad (A.4)$$

$$= 784 \times 0.019 = 14.896 \text{ N-m}$$

where $F_{steering}$ = fraction force

N = reaction of surface

μ = coefficient of friction

d_{swivel} = swivel distance

A.3 Computation for motor specifications

A.3.1 Motor for rolling

Required torque of the motor is computed as follows:

$$T_{rolling-motor} = T_{rolling} / gear_ratio \quad (A.5)$$

$$= 4.9 / 12 = 0.4083 \text{ N-m}$$

Required torque of the motor is 0.4083 N-m however we multiplied with safety factor of 2 so that the required torque of the rolling motor is 0.8166 N-m.

Required speed of the motor is computed as follows:

$$\text{Motor_rpm} = 60 (\text{required speed} / \pi d) \times gear_ratio \quad (A.6)$$

$$= 60 (1.2 / \pi \times 0.125) \times 12 = 2200 \text{ rpm}$$

where d = diameter of the wheel

A.3.2 Motor for steering

Required torque of the motor is computed as follows:

$$\begin{aligned} T_{steering_motor} &= T_{steering} / gear_ratio \\ &= 14.896 / 75 = 0.1986 \text{ N-m} \end{aligned} \quad (A.7)$$

Required speed of the motor

$$\begin{aligned} \text{Motor_rpm} &= 60 (\text{required speed} \times gear_ratio) \\ &= 60 (0.5 \times 75) = 2250 \text{ rpm} \end{aligned} \quad (A.8)$$

For simplicity, we use two motors with same specifications for driving and steering. The fabricated powered caster wheel architecture is shown in Figure A.1. There are two motors for the wheel, one is used for steering and the other is used for deriving. The wheel is non-deformable planner type. Therefore, the wheel has the capability of steering and driving independently. As can be seen from the figure, two motor amplifiers are mounted on the module to amplify the control signals from the PC.

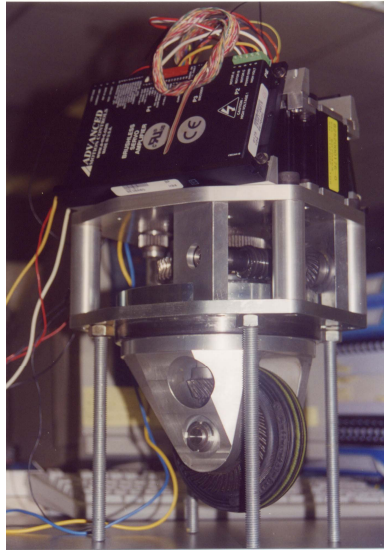
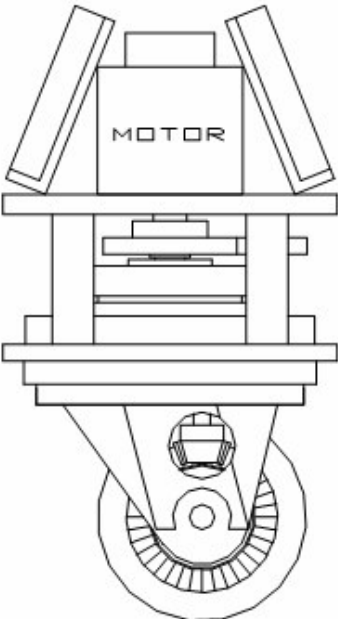
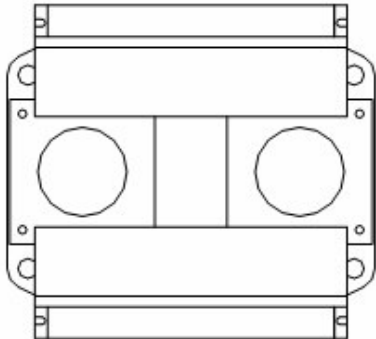
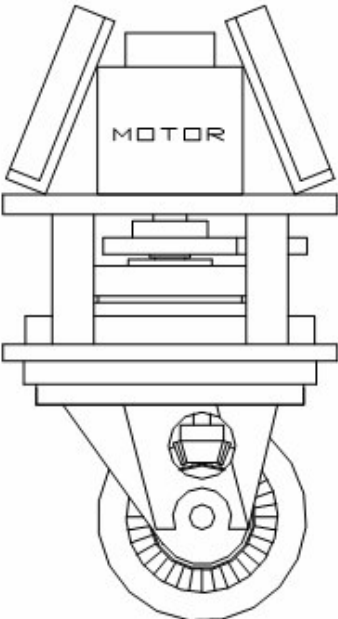
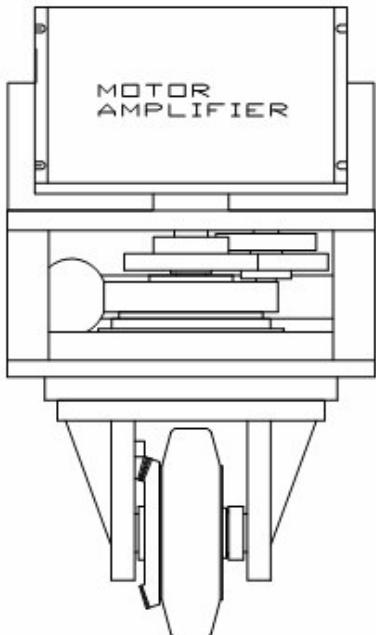


Figure A.1: Powered Caster Wheel Module

Appendix B

Drawings of Caster Wheel Module

1	1	2	3	1	4																					
RevNo	Revision note			Date	Signature																					
<p>POWERED CASTER WHEEL MODULE</p>																										
 <p>SIDE VIEW</p>			 <p>TOP VIEW</p>																							
 <p>FRONT VIEW</p>			 <p>MOTOR AMPLIFIER</p>																							
<table border="1" style="width: 100%; border-collapse: collapse;"> <tr> <th>Itemref</th> <th>Quantity</th> <th colspan="3">Title/Name, designation, material, dimension etc</th> <th>Article No./Reference</th> </tr> <tr> <td>Designed by MAUNG THAN ZAW</td> <td>Checked by</td> <td>Approved by - date</td> <td>Filename caster_wheel</td> <td>Date 18/03/01</td> <td>Scale</td> </tr> <tr> <td colspan="3" rowspan="2" style="text-align: center;">NATIONAL UNIVERSITY OF SINGAPORE</td> <td colspan="3" style="text-align: center;">POWERED CASTER WHEEL MODULE</td> </tr> <tr> <td style="text-align: center;">NO. PCWM1</td> <td style="text-align: center;">Edition 2</td> <td style="text-align: center;">Sheet A</td> </tr> </table>						Itemref	Quantity	Title/Name, designation, material, dimension etc			Article No./Reference	Designed by MAUNG THAN ZAW	Checked by	Approved by - date	Filename caster_wheel	Date 18/03/01	Scale	NATIONAL UNIVERSITY OF SINGAPORE			POWERED CASTER WHEEL MODULE			NO. PCWM1	Edition 2	Sheet A
Itemref	Quantity	Title/Name, designation, material, dimension etc			Article No./Reference																					
Designed by MAUNG THAN ZAW	Checked by	Approved by - date	Filename caster_wheel	Date 18/03/01	Scale																					
NATIONAL UNIVERSITY OF SINGAPORE			POWERED CASTER WHEEL MODULE																							
			NO. PCWM1	Edition 2	Sheet A																					

RevNo	Revision note	Date	Signature	Checked

Front View Dimensions:

- Overall width: 195
- Overall height: 200
- Top edge chamfer: 2.4456°
- Top edge radius: R59.1928
- Inner circle diameters: Ø120, Ø90, Ø73, Ø40, Ø32, Ø26, Ø18, Ø12, Ø6
- Bottom hole diameters: Ø25, Ø12, Ø6
- Bottom hole pattern: 6 X M6 COUNTERSUNK THRU
- Internal features: DEEP GROOVE BALL BEARING 6804 LLB, DEEP GROOVE BALL BEARING 6901 LLB

Side View Dimensions:

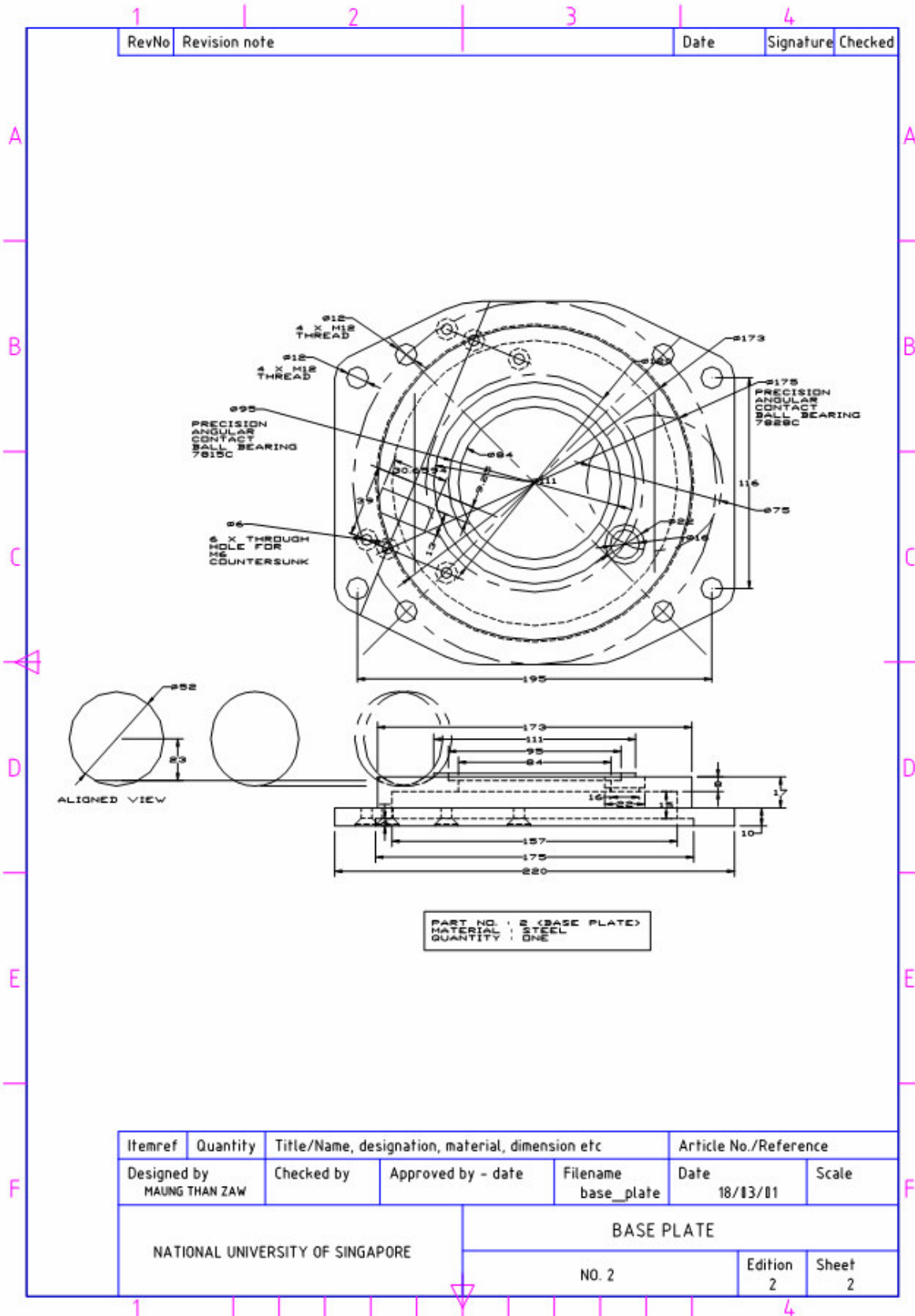
- Overall length: 220
- Overall thickness: 12
- Internal features: DEEP GROOVE BALL BEARING 6804 LLB, DEEP GROOVE BALL BEARING 6901 LLB

Part Information:

PART NO.: 1 (TOP PLATE)
MATERIAL: ALUMINIUM
QUANTITY: ONE

Itemref	Quantity	Title/Name, designation, material, dimension etc	Article No./Reference
Designed by MAUNG THAN ZAW	Checked by	Approved by - date	Filename top_plate
		Date 18/03/01	Scale

NATIONAL UNIVERSITY OF SINGAPORE	TOP PLATE	
	NO. 1	Edition 2 Sheet 1



RevNo	Revision note	Date	Signature	Checked

Top View:

- Overall diameter: $\phi 160$
- Inner circular feature diameter: $\phi 140$
- Distance from center to outer hole: $\phi 140$
- Distance from center to inner hole: $\phi 132$
- Outer hole diameter: $\phi 28$
- Inner hole diameter: $\phi 20$
- Feature: 8 X ANGULAR CONTACT BALL BEARING 7001
- Feature: 6 X M6 THREAD
- Feature: 7 X M8 THRU
- Dimension: 55.5 ± 0.75

Front View:

- Top flange width: 140
- Top flange thickness: 15
- Internal width: 132
- Bottom flange width: 132
- Bottom flange thickness: 12
- Height from base to top of bearing housing: 67.5
- Bearing housing internal diameter: $\phi 138$
- Total height: 99.0 ± 0.2
- Base diameter: $\phi 40$
- Base thickness: 24.6 ± 0.71
- Base hole diameter: $\phi 15$
- Base hole offset: 81.3 ± 0.18
- Base hole diameter: $\phi 57$
- Base hole diameter: $\phi 38$
- Dimension: 4.97 ± 0.06

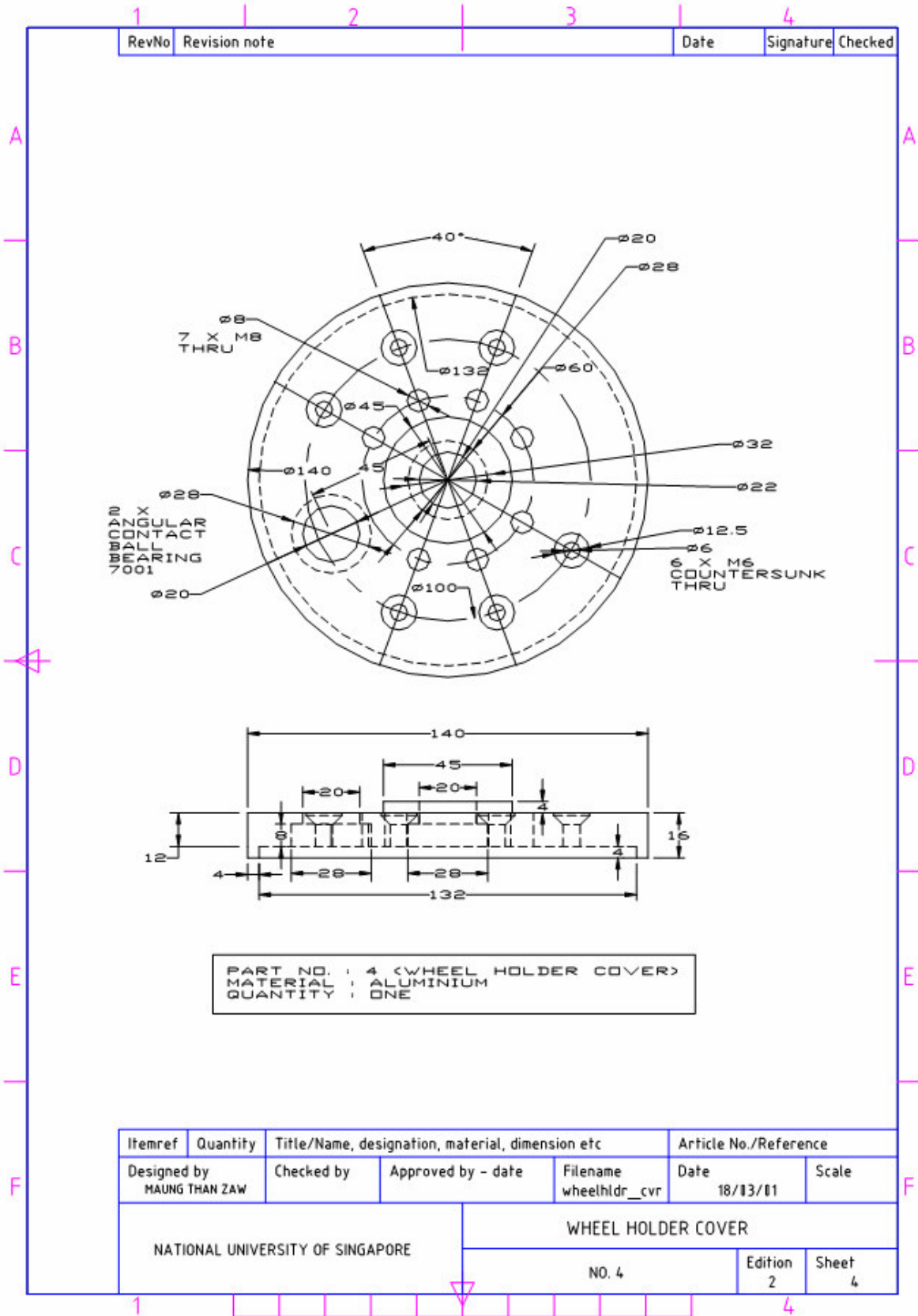
Side View:

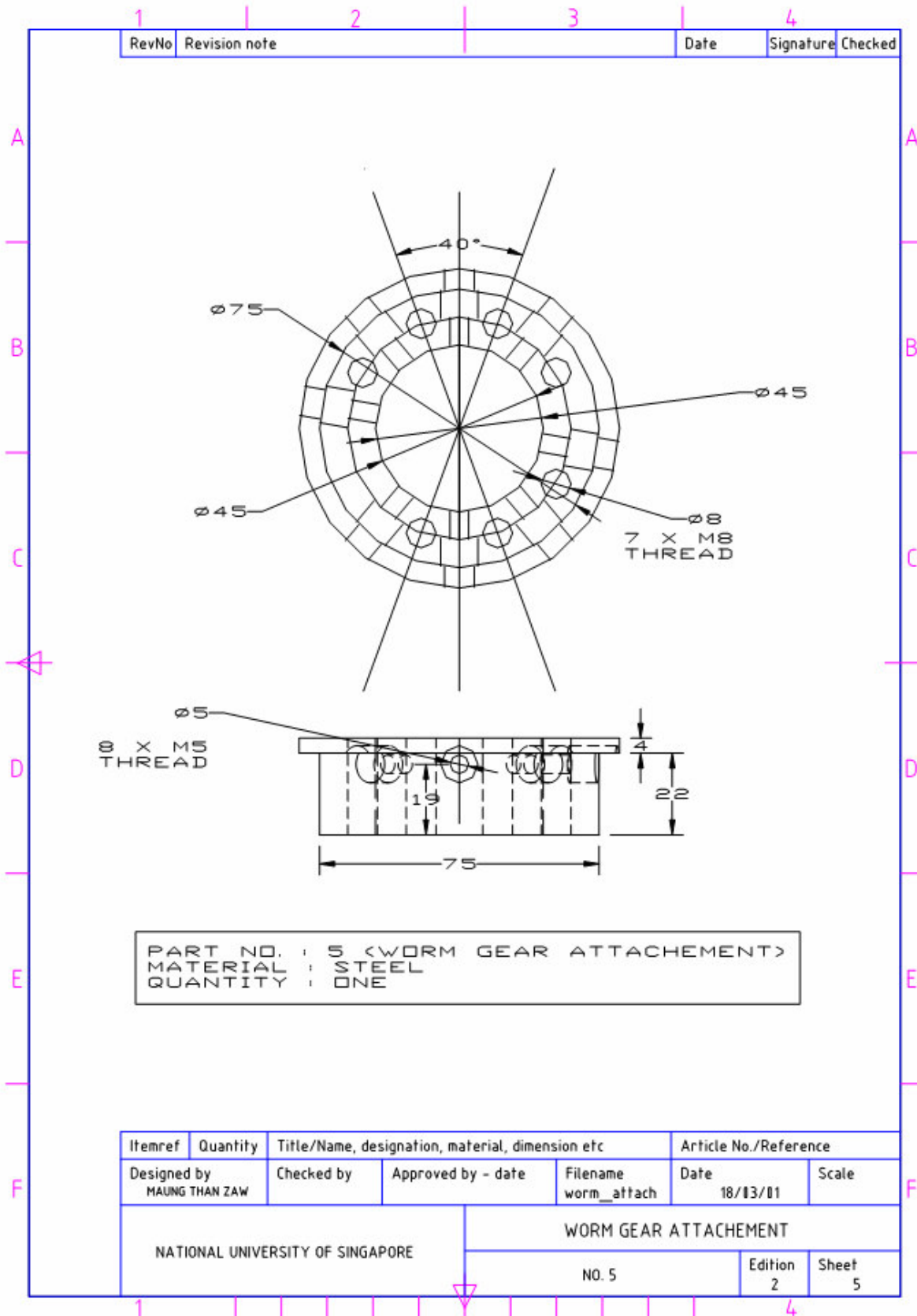
- Top flange width: 132
- Top flange thickness: 15
- Internal width: 132
- Bottom flange width: 132
- Bottom flange thickness: 12
- Height from base to top of bearing housing: 67.5
- Base width: 14

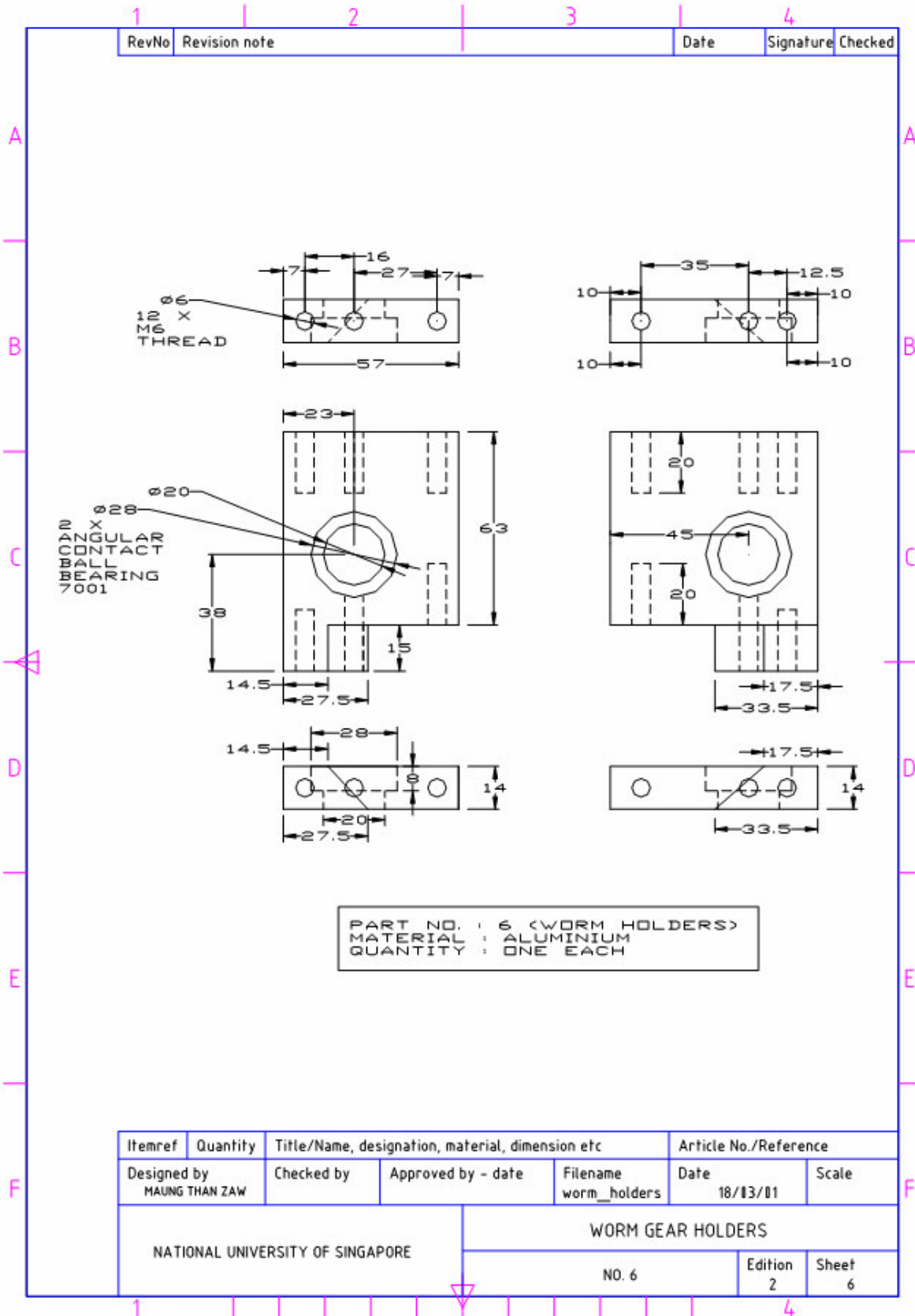
PART NO. : 3 (WHEEL HOLDER)
MATERIAL : ALUMINIUM
QUANTITY : ONE

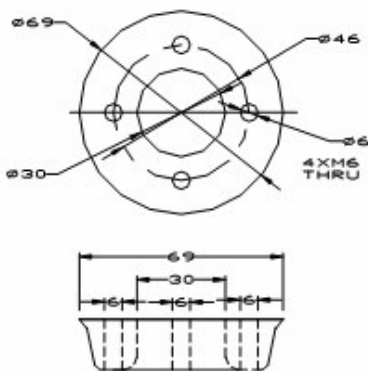
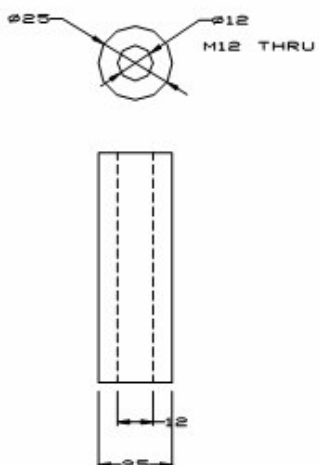
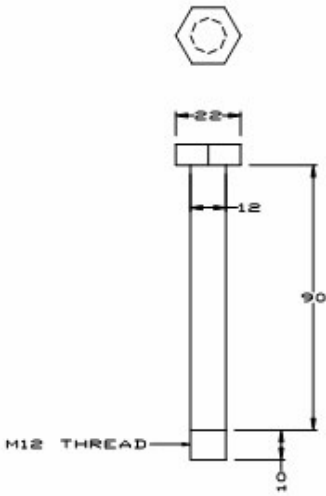
Itemref	Quantity	Title/Name, designation, material, dimension etc	Article No./Reference
Designed by MAUNG THAN ZAW	Checked by	Approved by - date	Filename wheel_holder
Date 18/13/01	Scale		

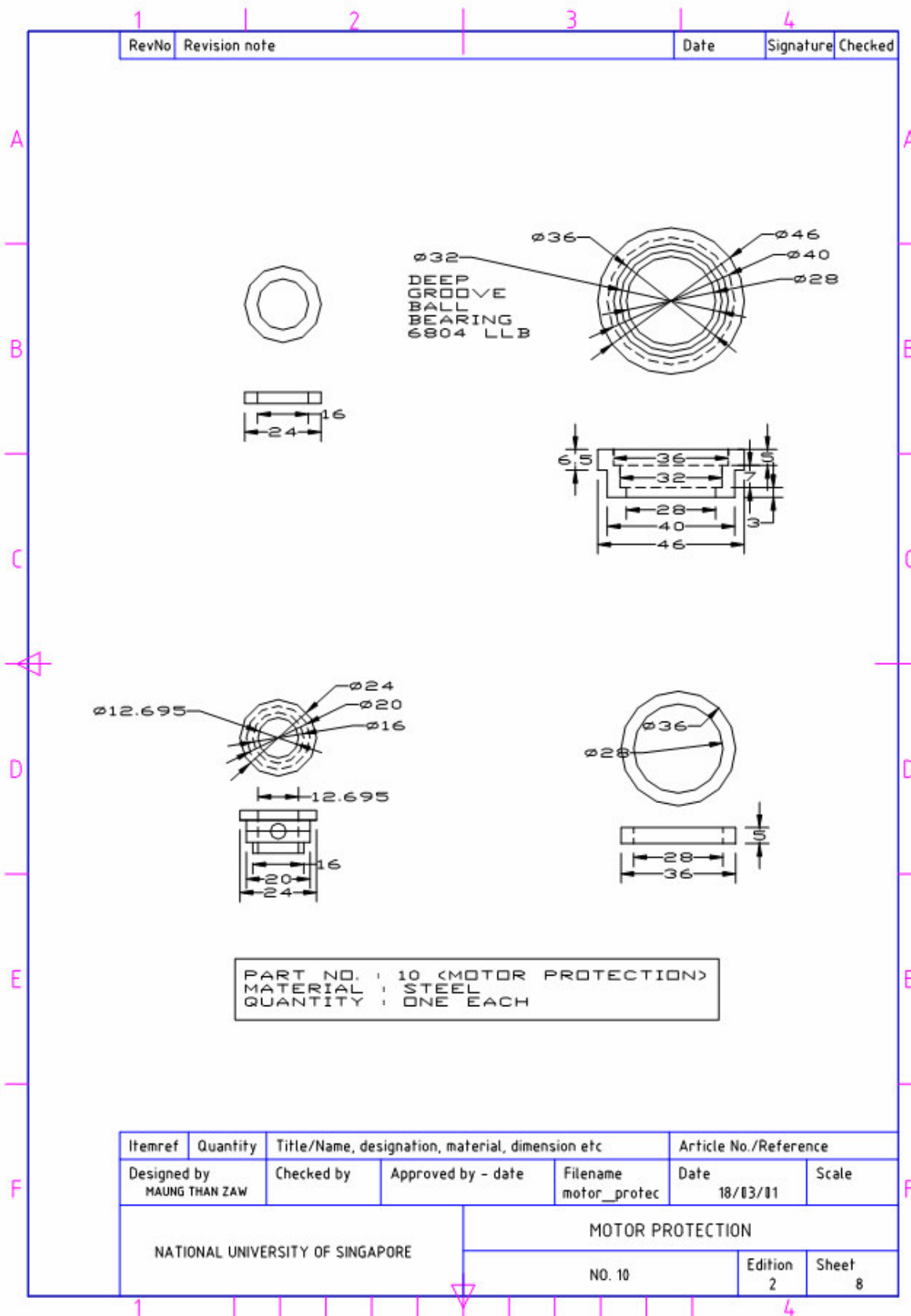
NATIONAL UNIVERSITY OF SINGAPORE	WHEEL HOLDER
NO. 3	Edition 2 Sheet 3

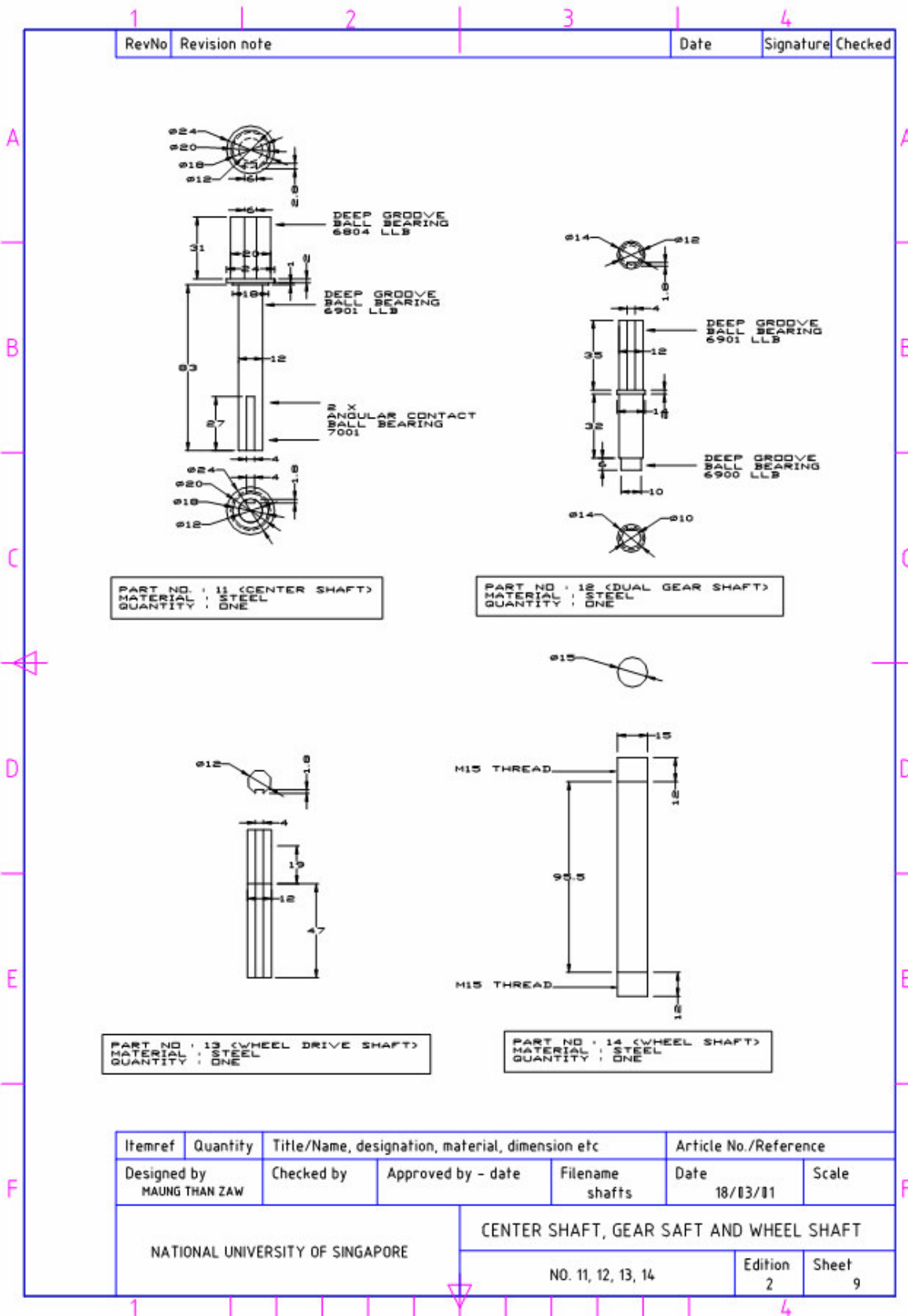






	1	1	2	3	1	4																			
	RevNo	Revision note			Date	Signature	Checked																		
A							A																		
B	<div style="border: 1px solid black; padding: 5px; width: fit-content; margin: 0 auto;"> PART NO. : 7 <WHEEL ATTACHEMENT> MATERIAL : ALUMINIUM QUANTITY : ONE </div>						B																		
C							C																		
D							D																		
E	<div style="display: flex; justify-content: space-around;"> <div style="border: 1px solid black; padding: 5px; width: 45%;"> PART NO. : 8 <PIPE> MATERIAL : ALUMINIUM QUANTITY : 4 </div> <div style="border: 1px solid black; padding: 5px; width: 45%;"> PART NO. : 9 <PIPE'S BOLT> MATERIAL : STEEL QUANTITY : 4 </div> </div>						E																		
F	<table border="1" style="width: 100%; border-collapse: collapse;"> <thead> <tr> <th style="width: 10%;">Itemref</th> <th style="width: 10%;">Quantity</th> <th style="width: 40%;">Title/Name, designation, material, dimension etc</th> <th style="width: 40%;">Article No./Reference</th> </tr> </thead> <tbody> <tr> <td>Designed by MAUNG THAN ZAW</td> <td>Checked by</td> <td>Approved by - date</td> <td>Filename wheelath_pipe</td> </tr> <tr> <td colspan="2"></td> <td>Date 18/03/11</td> <td>Scale</td> </tr> <tr> <td colspan="2" rowspan="2" style="text-align: center; vertical-align: middle;">NATIONAL UNIVERSITY OF SINGAPORE</td> <td colspan="2" style="text-align: center;">WHEEL ATTACHEMENT AND PIPE</td> </tr> <tr> <td style="text-align: center;">NO. 7, 8, 9</td> <td> Edition 2 </td> </tr> </tbody> </table>						Itemref	Quantity	Title/Name, designation, material, dimension etc	Article No./Reference	Designed by MAUNG THAN ZAW	Checked by	Approved by - date	Filename wheelath_pipe			Date 18/03/11	Scale	NATIONAL UNIVERSITY OF SINGAPORE		WHEEL ATTACHEMENT AND PIPE		NO. 7, 8, 9	Edition 2	F
Itemref	Quantity	Title/Name, designation, material, dimension etc	Article No./Reference																						
Designed by MAUNG THAN ZAW	Checked by	Approved by - date	Filename wheelath_pipe																						
		Date 18/03/11	Scale																						
NATIONAL UNIVERSITY OF SINGAPORE		WHEEL ATTACHEMENT AND PIPE																							
		NO. 7, 8, 9	Edition 2																						





1	2	3	4
RevNo	Revision note	Date	Signature
			Checked

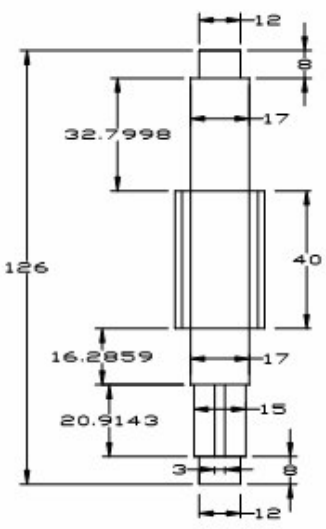
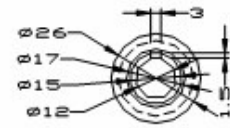
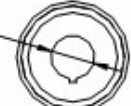
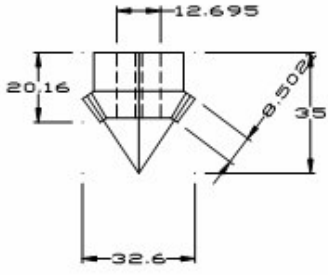
PART NO : 15 (CENTER SHAFT WASHER)
MATERIAL : STEEL
QUANTITY : ONE

PART NO : 16 (DUAL GEAR WASHER)
MATERIAL : STEEL
QUANTITY : ONE

PART NO : 17 (WHEEL DRIVE WASHER)
MATERIAL : STEEL
QUANTITY : FOUR

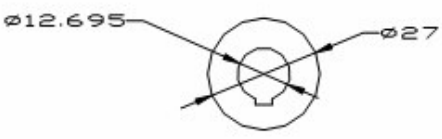
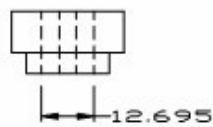
PART NO : 18 (WHEEL SHAFT WASHER)
MATERIAL : STEEL
QUANTITY : TWO

Itemref	Quantity	Title/Name, designation, material, dimension etc	Article No./Reference
Designed by MAUNG THAN ZAW	Checked by	Approved by - date	Filename washers
		Date 18/03/01	Scale
NATIONAL UNIVERSITY OF SINGAPORE		WASHERS	
		NO. 15, 16, 17, 18	Edition 2
		Sheet 10	

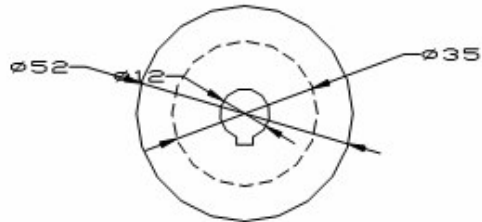
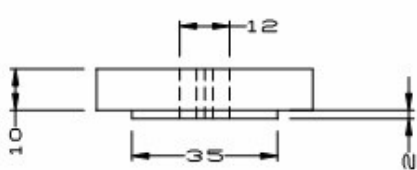
1	1	2	3	1	4
RevNo	Revision note			Date	Signature Checked
<div style="border: 1px solid black; padding: 5px; width: fit-content; margin: 0 auto;"> SECONDARY MACHINING FOR PART NUMBER KWG2-R1 </div>					
<div style="border: 1px solid black; padding: 5px; width: fit-content; margin: 0 auto;"> SECONDARY MACHINING FOR PART NUMBER MBSA1.5-2030L </div>			  		
Itemref		Quantity	Title/Name, designation, material, dimension etc		Article No./Reference
Designed by MAUNG THAN ZAW		Checked by	Approved by - date	Filename secondary2	Date 18/03/01
NATIONAL UNIVERSITY OF SINGAPORE			SECONDARY MACHINING FOR WORM SHAFT, BEVEL		
			NO. S3, S4		Edition 2

	1	2	3	4
	RevNo	Revision note	Date	Signature
				Checked

SECONDARY MACHINING
 FOR PART NUMBER
 MSGB1-25

SECONDARY MACHINING
 FOR PART NUMBER
 MSGA1-50

Itemref	Quantity	Title/Name, designation, material, dimension etc	Article No./Reference
Designed by MAUNG THAN ZAW	Checked by	Approved by - date	Filename secondary3
			Date 18/03/01
			Scale
NATIONAL UNIVERSITY OF SINGAPORE		SECONDARY MACHINING FOR SPUR GEAR 1 & 2	
		NO. S5, S6	Edition 2
			Sheet 13